J. Magn. Soc. Jpn., **41**, 108-126 (2017)

<Review>

Development of Media Nanostructure for Perpendicular Magnetic Recording

Masaaki Futamoto and Mitsuru Ohtake

Faculty of Science and Engineering, Chuo University, *1-13-27 Kasuga, Bunkyo-ku, Tokyo 112-8551, Japan*

The review covers the research and development of perpendicular media nanostructure focusing on the recording layer. The recording layer material includes the Co-alloys with hcp structure, the magnetic multilayers, and the alloys with ordered structures that have high magneto-crystalline anisotropies (K_u). The technologies of underlayer or interlayer for aligning the easy magnetization axis of magnetic crystal grain perpendicular to the film plane are briefly reviewed including the high K_u magnetic materials for future recording media.

Observations of compositional and magnetization structures in sub-µm scale have played important roles in improving the recording layer. Typical data on these characteristics are explained in relation to the media structure improvements. Considering that high K_u magnetic materials will be employed in future recording media, basic experimental results related in controlling the easy magnetization axis and in keeping the surface flatness of $L1_0$-ordered magnetic materials are explained. Future possibilities for increasing the areal density beyond 1 Tb/in^2 by improving the magnetic material and the nanostructure of recording layer are also discussed.

Key words: perpendicular magnetic recording, thin film media, nanostructure, compositional structure, magnetization structure, Co-alloy, ordered alloy, multilayer, high K_u magnetic material, epitaxial growth

1. Introduction

The areal density of hard disk drive (HDD) is now around 1 Tb/in^2 which is 5×10^8 of the areal density employed in the world-first HDD developed in 1956 (2 Kb/in^2, 100 bits/in, 20 tracks/in). Now all the HDDs are based on the perpendicular magnetic recording (PMR) technology that was invented by Prof. Iwasaki in 1976 [1]. PMR involves nearly 30 years of research and development before the technology started to be used in commercial HDDs in 2005 by replacing the conventional longitudinal magnetic recording (LMR) technology. Table 1 shows the brief history of research and development until the shipment of PMR-HDD, listed by keywords from a viewpoint of perpendicular magnetic recording media technology [2]. Although the PMR research and development attracted much attention in the magnetic recording community from late 1970's to early 1980's, there was a dip period of 10 - 15 years, from middle 1980's to late 1990's which is shown as the background shadow in the table, with low activities in the academic and the HDD-related communities. This was partially because that there were a couple of engineering issues [3-6] which needed to be solved before applying PMR to the commercial HDDs, and mainly due to that it was considered at that time possible to increase the areal density with the conventional LMR. The high cost for production facilities in changing the recording scheme could be an additional reason for the industries. However, as the areal density increased beyond 10 Gb/in^2, the signal decay problem associated with thermal instability with LMR [7-9] gradually narrowed the allowance in HDD product design. Triggered by a high-density magnetic recording demonstration using PMR[10] and by the developments of PMR media technology which solved the engineering issues[11-18], activities toward realization of HDD products based on PMR emerged drastically in the magnetic recording community from the year around 2000 and the first PMR-HDD product was shipped in 2005 with an areal density of 133 Gb/in^2 [19, 20]. The areal density of PMR-HDD increased since then about 10 times and the technologies for achieving 5 - 10 Tb/in^2 areal densities are investigated in the cutting edge research laboratories[21, 22].

In the PMR technologies, the recording media and the writing head are different from those for conventional LMR whereas other technologies like the reader head and the mechanical positioning have much in common. The present paper reviews the development of PMR media technology focusing on the nanostructure of Co-alloy recording layer. To further increase the areal density well beyond 1 Tb/in^2, magnetic materials with the magneto-crystalline anisotropy (K_u) higher than those of Co-alloys need to be employed. Some of the basic key points in tailoring the high K_u magnetic thin films are also briefly reviewed.

2. Technologies in controlling the structure of Co-alloy recording layer

When a CoCr-alloy magnetic material with hcp structure is deposited on a substrate, a texture growth proceeds with the *c*-axis direction perpendicular to the substrate surface[23], where the *c*-axis is the easy magnetization of Co-alloy crystal with an hcp structure. However, crystal grains with different growth orientations coexist in the early stage of film growth near the substrate as shown in the cross-sectional transmission electron microscope image of Fig.1 (a) [24].

Table 1 Research and development history of perpendicular magnetic recording media technologies [2)]

Year	**1975**	**1980**	**1985**	**1990**	**1995**	**2000**	**2005**	**2010**
Areal density	5 Mb/in^2	10 Mb/in^2		100 Mb/in^2	1 Gb/in^2	10 Gb/in^2	100 Gb/in^2	500 Gb/in^2
Recording layer	CoCr			CoCrTa	CoCrPt	CoPtCr + Oxides		
Technologies ・Thin film media technology	**PMR invention by Prof. Iwasaki** (Tohoku Univ., 1976) CoCr-alloy PMR media (Tohoku Univ., 1978) SUL noise observation (Hitachi, 1984) *c*-axis control by underlayer (Hitachi, etc. 1985) PMR media, *L1₀*-FePt (AIT, 1997) SUL noise reduction (JVC, 1996) Improved underlayers (Hitachi, 1996-1997) Media noise reduction (Hitachi, 1997-1998) High *Hc*, high *Mr/Ms* media (Hitachi, 1998) CoPtCrO high *Hc*, high *Mr/Ms* media (Toshiba, 2000) Improved SUL (Hitachi & many companies, 2000) CGC media (IBM & Tohoku Univ., 2002) Improved Ru-underlayer (Fujitsu, etc., 2005 -) PMR media, SmCo5 (Shinshu Univ. Waseda Univ. etc., 2004)							
・Structure analysis technology	Cross-sectional TEM (Hitachi, etc., from around 1984) Segregation structure observation by TEM using chemically etched sample (NTT, 1984-1994) Magnetization structure observation by E-holography (Hitachi, 1986-1987) Magnetization structure observation by MFM (Hitachi, etc., from around 1992) Compositional segregation observation by AP-FIM (Tohoku Univ., 1992-1994) Compositional segregation observation by EELS and EDX TEM (Hitachi, from 1995) Basic magnetic properties determined using Co-alloy single-crystals, *Ku*, *α*, etc. (Hitachi, Tohoku Univ. from 1996)							
Events	Drastic growth of PMR R&D (Japan, US, Europe, 1976 - 1985) Tribology-related problems, PMR-floppy-disk (Many companies, middle '80s) Pulling out from Ba-ferrite floppy PMR media business (Toshiba, late '80s) US HDD companies shifted to LMR, Japanese companies followed (middle-late '80s) Giving-up PMR-HDD business (Censtor, Fujitsu,1991-1993) Negative report on PMR (IBM, 1998) Thermal stability problem prediction (CMU, 1994) 52.5 Gb PMR demonstration (Hitachi, 2000) Commercialization of PMR-HDDs (Toshiba, 2005)							

Areal density: the areal density of commercialized HDD and therefore the values before the year 2005 are those of LMR-HDDs.
Recoding layer: the typical recording layer material studied for PMR media. There were many variations, for example, CoCrPt*X* (*X*=Ta, Nb, Si, B, etc.).
Background shadow: it shows the R&D activities of PMR in the world. There was a dip period of 10 - 15 years from middle 80s to late 90s.

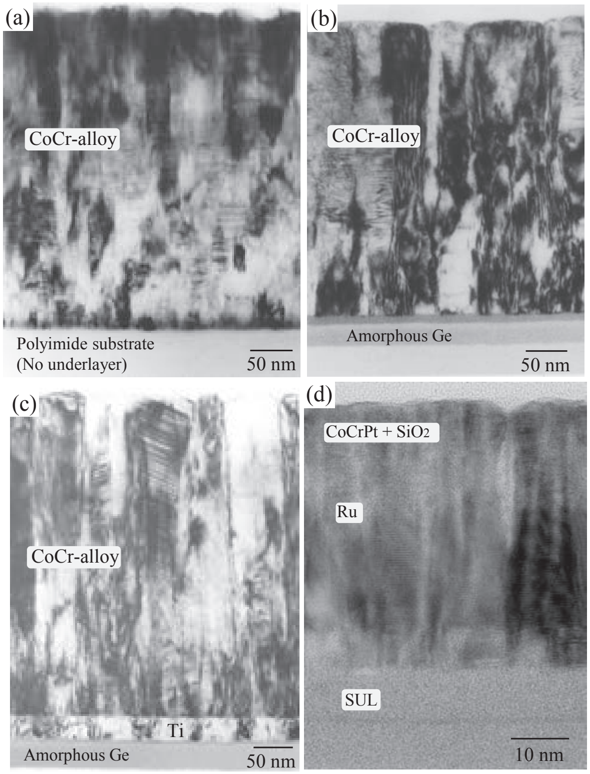

Fig. 1 TEM micrographs of PMR media [2)]. The numbers in parentheses are the years of observation or publication.
(a) CoCr-alloy thin film deposited on polyimide substrate with no underlayer, (1985). (b) CoCr-alloy thin film deposited on amorphous Ge underlayer, (1985). (c) CoCr-alloy thin film deposited on Ti/Ge composite underlayer, (1988). (d) CoCrPt + SiO_2 thin film deposited on Ru layer, (2008).

The presence of initial growth region is undesirable for PMR media, since it deteriorates the perpendicular magnetic anisotropy[25, 26)]. To enhance the crystal nucleation with the *c*-axis perpendicular to the substrate surface, underlayer materials were investigated around middle 1980's, and the materials like hcp-Ta [27)], hcp-Ti [28, 29)], amorphous-Ge [30)] were found suitable for this purpose. The underlayer has to offer a surface condition for Co-alloy crystal to nucleate with the basal (0001) parallel to the surface through hetero-epitaxial growth. Such nucleation of Co-alloy crystal is also possible on a neutral-type surface that promotes free nucleation of Co-crystal, where the (0001) basal plane with the lowest surface energy tends to be favored parallel to the nonmagnetic underlayer surface. Underlayer materials were then extended to nonmagnetic hcp-CoCr [31, 32)], hcp-Ru [30, 33)], fcc-Au, fcc-Al [34)], fcc-Pt [35)], etc. and dual-underlayer structures; Ti/Ge [36)], CoCr/TiCr [37, 38)], Co_3O_4/Pt [35)], Pt/Ti [39)], Pd/Ti [40)], CoCrRu/TiCr [41)], Ru/Ta [42, 43)], Ru-oxide/Ru [44)], etc. for the preparation of PMR media. Figures1 (a)-(d) show the variation in cross-sectional structure of CoCr-alloy film by employing amorphous Ge, hcp-Ti/Ge, and hcp-Ru underlayers [2)]. The *c*-axis of CoCr-alloy crystal is well controlled perpendicular to the substrate surface, and the crystal grain diameter distribution is narrowed for the films with hcp-Ti/Ge and Ru underlayers. The distributions of crystal grain diameter for Ti and Ru crystals are relatively narrow when the underlayer materials are deposited on neutral-type amorphous layers. The perpendicular magnetic anisotropy was enhanced greatly by introducing such underlayers.

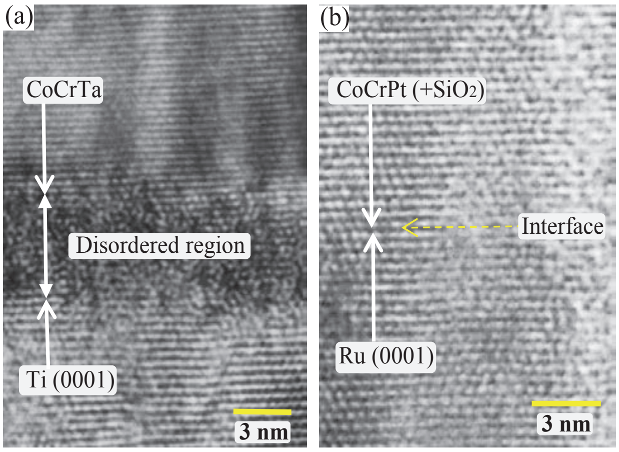

Fig. 2 Cross-sectional high-magnification TEM micrographs showing the interface between recording layer and underlayer [2].
(a) CoCrTa film deposited on Ti (0001) underlayer, (1991) [47].
(b) CoCrPt-SiO$_x$ thin film deposited on Ru (0001) underlayer, (2008).

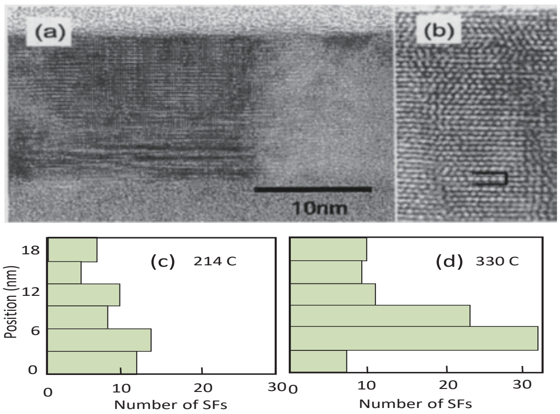

Fig. 3 Distribution of stacking faults (SFs) in CoCrPt recording layer (2002).
(a) Cross-sectional TEM image, (b) high-resolution image showing an example of stacking fault, (c) SF distribution along a CoCrPt layer grown at a substrate temperature of 214 °C, (d) SF distribution along an another CoCrPt layer grown at 330 °C. The structure is CoCrPt(18 nm)/NiTaZr/Glass substrate [52].

With increasing linear recording density, the perpendicular coercivity must be increased while the recording layer thickness needs to be reduced to enhance the writing efficiency of a recording head. In the nearly 30 years since the PMR invention in 1976, the recording layer material varied from a binary CoCr-alloy to ternary or more complex alloys of CoCrTa, CoCrPt, and CoPtCr + X (X = Ta, Si, Nb, B, oxides). The shift was necessary for increasing the K_u value of recording layer, which was directly related with increasing the perpendicular coercivity. When the layer thickness was decreased for Co-alloy recording layer materials to be less than 50 nm, a notable decrease in perpendicular coercivity was observed and the decrease depended on the underlayer material [12, 45, 46]. Careful examinations of the interface between the Co-alloy recording layer and the underlayer revealed that there was an atomically disordered region of a few nanometers around the interface [38, 46, 47]. Figure 2(a) shows the TEM image of initial growth region observed for a CoCr-alloy film deposited on a Ti underlayer [2, 47]. The formation of disordered region was partially due to a large lattice misfit of about 15% between the CoCr-alloy magnetic material and the Ti underlayer, and also due to an inter-diffusion of elements which was caused during a deposition process at an elevated substrate temperature of around 250 °C. An introduction of nonmagnetic layer with hcp-crystal structure such as CoCr$_{35}$, CoCr$_{25}$Ru$_{25}$, or Ru, which possessed a lattice constant close to that of the Co-alloy recording layer material, was proved effective in forming a sharp elemental interface while keeping an epitaxial relationship between the two layers [12, 46-50]. Compositional variations across the interface were investigated by using a TEM equipped with an EDX, and it was confirmed that the distance of elements diffusion from the underlayer toward the magnetic layer was very small, less than the electron-beam diameter of 2 nm employed in the EDX analysis [49]. An example of CoCrPt (+SiO$_2$) magnetic layer deposited on a Ru layer is shown in Fig. 2(b). Formation of atomically sharp interface was proved effective in maintaining high perpendicular coercivities of PMR media for reduced magnetic layer thicknesses.

Another origin that deteriorates the perpendicular magnetic anisotropy is stacking faults (SFs) in the hcp-Co-alloy crystal. When a SF exists in an hcp-Co-alloy crystal, the local atomic stacking sequence becomes similar to that of fcc-structure. The magnetic anisotropy of fcc-Co with cubic symmetry is one magnitude lower than that of hcp-Co [51]. Perpendicular coercivity decreases when SFs exist in the crystals of hcp-Co-alloy recording layer. Distribution of SF was investigated for the Co-alloy recording layers using a high-resolution TEM and it was revealed that it depended on the process condition like substrate temperature, deposition rates of recording layer, underlayer, and intermediate layer materials. An example of such analysis on the distributions of SF along CoCrPt crystal columns is shown in Fig. 3 [52]. The recent investigations on CoPt-alloy materials have shown that the atomic attacking sequence is also influenced by the average number of valence electrons of alloy material, and the SF density decreases when the number approaches to a certain value through adjustment of compositional alloy elements [53]. In PMR media productions, the media structure and the process conditions are carefully controlled to lower the SF density in the recording layer.

3. Compositional structure of recording layer

Compositional fluctuations of Co and Cr in vacuum

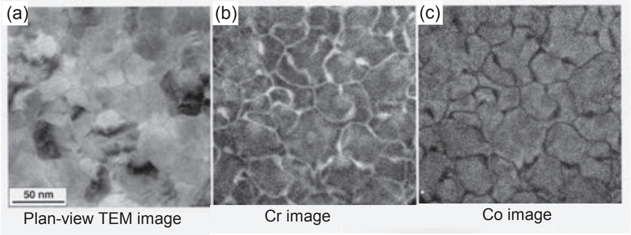

Fig. 4 Cr and Co distributions in a CoCrTa perpendicular medium deposited at 230 °C investigated by EELS-TEM (1996), (a) plan-view TEM image, (b) Cr distribution map, and (c) Co distribution map [66, 67].

evaporated or sputter deposited CoCr alloy thin films were studied initially from a viewpoint to explain the magnetic property differences between thin film and bulk samples, and they were investigated by using NMR [54], FMR [55], chemical etching [56-58], and TEM equipped with an analytical facility in middle to late 1980's [59, 60]. It was in late 1980's when a relation between the non-magnetic Cr concentration in LMR-CoCrTa recording layer and the medium noise property was investigated and it was demonstrated that a Cr-rich CoCrTa thin film medium showed a lower noise property [61-65]. Magnetic crystal grain isolation while controlling the diameter in the recording layer was realized necessary for high-density perpendicular magnetic recording to increase the coercivity, the recording resolution and to decrease the medium noise. Magnetic decoupling and/or reduction of interaction between the neighboring magnetic crystal grains were achieved by enhancing segregation of nonmagnetic metallic elements (Cr, Ta, etc.) toward crystal grain boundaries. The technology has been improved, from around the year 2000, by employing a technique of nonmagnetic material (SiO_x etc.) precipitation along the magnetic crystalline grain boundaries, which is based on a physical segregation of two different phases, metallic magnetic and nonmagnetic amorphous materials, during a film formation process. Figure 4 shows the Cr and the Co distributions visualized for a Co-17at%Cr-3at%Ta PMR medium, where nonmagnetic Cr atoms are strongly segregated near the grain boundaries and are depleted inside the crystal grains [66, 67]. The distribution of Co atom is showing an opposite tendency. When the Cr concentration in a CoCr-alloy material exceeds 30 at. %, the material becomes nonmagnetic at room temperature.

Employment of a sputter deposition system with ultra-high-vacuum background pressure [37, 68] and with a high purity Ar sputtering gas were shown effective in enhancing nonmagnetic elements segregation toward the magnetic crystalline grain boundaries [69]. The residual gasses in a sputter deposition chamber such as water-vapor deteriorate the perpendicular magnetic properties through selective reaction with active Cr atoms forming oxides and/or hindering segregation within the magnetic crystal grains [70]. Strong Cr segregation around the magnetic crystal grains weakens or decouples the direct magnetic exchange between the neighboring magnetic crystal grains, thus contributing to a reduction of medium noise, an increase of coercivity, and an increase of recording resolution.

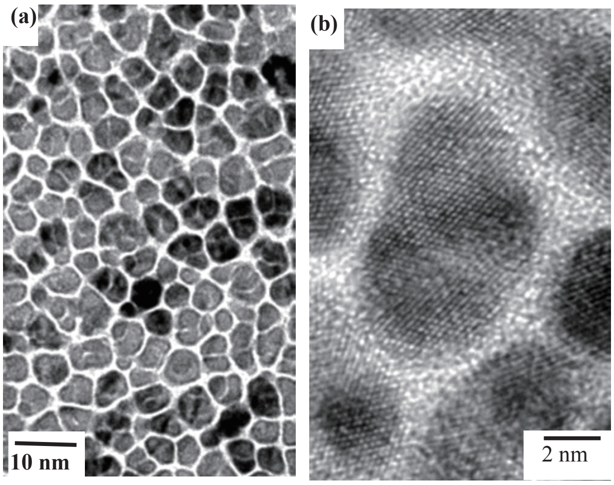

Fig. 5 Plan-view TEM images of CoCrPt-SiO_x perpendicular medium, (2008). (a) TEM image showing the magnetic crystal grains isolated by thin oxide layer and (b) high magnification TEM image [88].

The high-density magnetic recording demonstration using PMR in the year 2000 [10] was performed by employing CoCr-alloy perpendicular media with enhanced Cr segregation around the magnetic crystal grain boundaries [48, 71]. Although the low noise and the high recording resolution properties were achieved with the media, time dependent decays of recorded signals were observed particularly at low linear densities [72. 73]. This was because that the remanent magnetization M_r was lower than the saturation magnetization M_s, $M_r/M_s<1$, where a demagnetization field was working in an opposite way to the recorded bit direction and caused a time-dependent thermal decay in the recorded information. Although the necessity of media preparation with squareness, $M_r/M_s = 1$, was realized for suppressing such time-dependent thermal decay of signal, the M_r/M_s values of CoCr-alloy media were less than 1 up to the late 1990's [71-73]. Magnetic multilayers composed of Co and noble metals (Co/Pt, Co/Pd) were, on the contrary, known to be tuned easily to possess the value, M_r/M_s, to be 1, and they were investigated as practical magnetic recording media [74, 75-79]. However, the multilayer structure which needed complicated film deposition processes was one of the drawbacks of media production. A novel technology in increasing the M_r/M_s to be nearly unity while achieving a magnetic grain isolation was developed from the year around 2000. The technology introduced oxygen into the Co-alloy thin films, which had a similarity with that of the magnetic tape technology that employed low noise Co-CoO recording layers [80-82].

Addition of oxygen or oxide to a CoPt or a CoCrPt magnetic material during the sputter deposition process

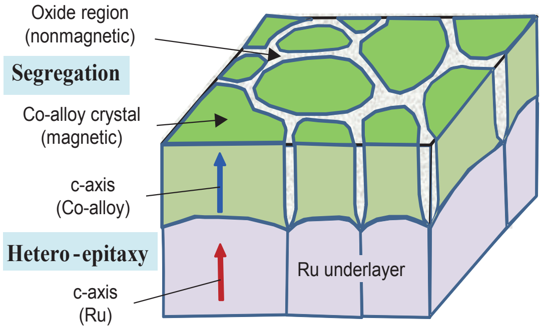

Fig. 6 Structure model of CoCrPt-SiO$_x$ perpendicular medium. Co-alloy magnetic crystals are epitaxially grown on *c*-axis oriented Ru crystals. Thin oxides are separating magnetic interaction between Co-alloy crystal grains[126].

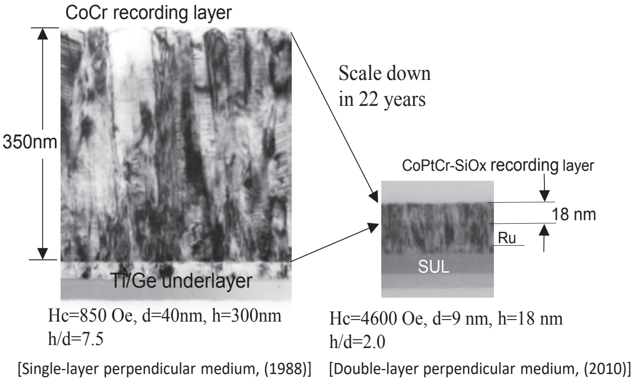

Fig. 7 Comparison of perpendicular recording media. Recording layer height (*h*) and grain diameter (*d*) have been reduced greatly while perpendicular coercivity has been increased in the 22 years from 1988 to 2010 [2].

showed a drastic effect in enhancing the magnetic crystalline grain isolation. The technology was first applied to CoPt media in 1994 [83] and then to CoPtCr media in 2000 [84]. Perpendicular magnetic properties including the coercivity and the squareness (M_r/M_s) were greatly improved by addition of oxides like SiO$_x$, which were carried out in the early years of this century, accelerated the realization of commercial PMR HDDs [85, 86]. A plan-view TEM image of CoCrPt-SiO$_x$ perpendicular medium is shown in Fig. 5. The compositions of CoCrPt-SiO$_x$ perpendicular media were studied by employing a TEM equipped with an EDX facility, where the local compositions of 1 - 2 nm in diameter area could be determined. With this type media, the magnetic crystal grains of sub-10 nm in diameter are separated by oxide-based grain boundaries of around 1 nm width and this type granular media have been used as the recording media of commercial HDDs. The high magnification TEM image clearly indicates that most of the grains are single crystals and the grain boundary structure is amorphous. The grain boundary compositions were investigated, and it was found that not a small amount of metallic elements other than Si were included in the grain boundaries [87-89]. The metallic elements (Co, Cr, Pt, etc.) are considered to be dissolved in the matrix SiO$_x$ through forming oxides like CoO and Cr$_2$O$_3$. The composition indicates that the grain boundary is non-magnetic and the thin oxide layer is drastically reducing the magnetic interaction between the neighboring magnetic crystal grains. A model of PMR medium[126], based on the structural and the compositional investigations, is depicted in Fig. 6. Various nonmagnetic materials such as C [90], SiO$_2$ [91], TiO$_2$ [92], Ta$_2$O$_5$ [93]), etc. have been investigated for magnetic crystal grain isolation of hcp-Co-alloy materials. Although any nonmagnetic material that segregates along the grain boundary during a sputter deposition process is possible for magnetic crystal grain isolation, practical conditions in a mass-production of recording media including easy handling, homogeneity of nanostructure, reproducibility in the fabrication, etc. are considered. As a result, SiO$_x$-based oxide materials are now widely employed in the commercial PMR media fabrication.

4. Tuning the nanostructure of recording layer

Figure 7 compares the cross-sectional TEM micrographs of Co-alloy PMR media developed in middle 1980's and in 2010 showing the development of nanostructure in over a quarter century. While achieving a drastic scale down in the length and the width of *c*-axis oriented Co-alloy crystal grain, the medium coercivity was increased from around 0.8 kOe to be larger than 4 kOe by controlling the alloy composition, the underlayer material, and the processing condition, all of which were inevitable in increasing the areal density. The PMR media used in commercial HDDs employ the double magnetic layer structure consisting of a semi-hard magnetic recording layer stacked on a soft magnetic underlayer, which is the basic PMR structure proposed by Prof. Iwasaki [1]. Until late 1990's, the Co-alloy recording layer was deposited directly on a thick soft-magnetic underlayer of crystalline Fe-Ni [94, 95], amorphous Co-Zr-Nb [11, 96], etc. However, a series of research has shown that the medium noise can be reduced by introducing a thin nonmagnetic layer between the soft magnetic underlayer and the semi-hard recording layer, where the nonmagnetic layer is now defined as an intermediate layer since the soft magnetic layer is called as "underlayer" in the double layer structure [97]. Such magnetic decoupling between the two magnetic layers was effective in preventing a transmission of short wave length noise caused in the soft magnetic underlayer [98-100].

The introduction of nonmagnetic interlayer offered another positive effect in controlling the structure of recording layer independently from that of soft magnetic underlayer (SUL), where a smaller thickness SUL was desirable in achieving an efficient magnetic writing with a single-pole writing head. As explained in the previous section, the nanostructure of recording layer must be controlled simultaneously in the crystal orientation, the grain diameter, as well as the separation between magnetic grains with a presence of thin nonmagnetic layer. Dual layer structures of hcp-Ru/Ta [42, 43], hcp-Ru/Ni-W, or even more complicated stacked structures [101, 102] were employed as the intermediate layer, where the first layer of Ta or Ni-W provided a surface condition that promoted free nucleation of hcp-Ru crystal with the (0001) basal plane, energetically most stable plane, parallel to the surface. A sputter deposition consisting of low Ar pressure deposition followed by high Ar pressure deposition for the Ru layer preparation was employed to produce an intermediate layer with the *c*-axis oriented dome-like Ru crystal grains which were effective in enhancing nonmagnetic SiO_x segregation around the Co-alloy magnetic crystal grains [101, 102]. The Ar pressure for sputtering is known to give an influence on the topological nanostructure of deposited film [103].

Since a PMR medium is used in combination with a magnetic head in an HDD system, a careful adjustment in the magnetic property of recording layer is carried out through an optimization not only from the intermediate layer but also for the Co-alloy composition, the nonmagnetic material for magnetic crystal separation, the sputter deposition condition, etc. Magnetic property control along the thickness of Co-alloy recording layer by employing a compositional gradient technique or a deposition of layers with different properties was used for tuning the medium property suitable for high areal density PMR [101, 104, 105].

5. Recorded magnetization structure

Magnetization structure observation gives valuable information for the investigations on the inter-relationship between medium structure and recording characteristics of recording resolution and medium noise. Bitter method is the easiest technique and it was applied in middle 1980's to investigate the effect of *c*-axis orientation of CoCr-crystal grains on perpendicular magnetization. An example is shown in Fig. 8. The Bitter observation from the top and the bottom sides of recording medium showed that a stronger perpendicular magnetization was realized for a medium with higher *c*-axis orientation [106]. More quantitative estimation of perpendicular magnetization was later carried out in 1986 - 1987 by using the electron holography technique[106-108]. Figure 9 shows the electron holography images of CoCr-alloy media with different degrees of *c*-axis orientation observed for the media cross-sections. The data showed that a perpendicular magnetization at 300 kFCI (bit length = 80 nm) recording was achieved through the whole film thickness of 200 nm for the highly *c*-axis oriented CoCr medium sample, indicating that the medium structure, particularly the alignment of easy magnetization orientation, was giving a very strong influence in achieving a high linear density magnetic recording.

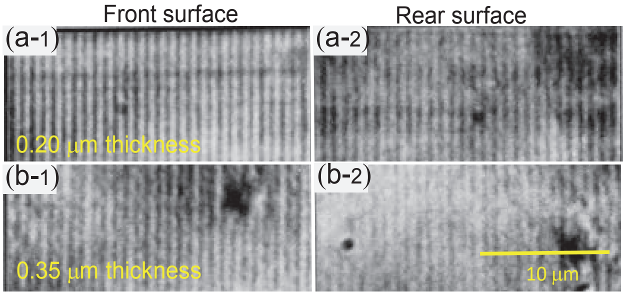

Fig. 8 Optical microscope images of recorded magnetization observed by Bitter method. CoCr perpendicular thin film media with thicknesses of 0.20 and 0.35 μm were observed from the front and the rear surfaces, (1987).
Bitter images of 20 kFCI recording on a 0.20 μm thick CoCr/Ge perpendicular thin film observed from (a-1) top and (a-2) rear surfaces.
Bitter images of 20 kFCI recording on a 0.35 μm thick CoCr/Ge perpendicular thin film observed from (b-1) top and (b-2) rear surfaces [106].

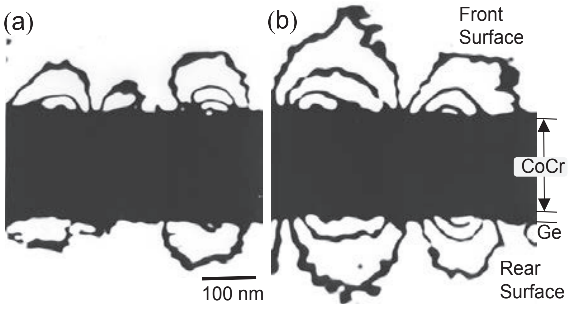

Fig. 9 Electron holography images of magnetization recorded at 300 kFCI observed for cross-sectional CoCr perpendicular media samples without and with Ge underlayer, (1987).
Magnetic leakage flux intensity is different between the front and the rear surfaces for a CoCr film without underlayer (a).
Magnetic leakage flux intensity is similar at the front and the rear surfaces, indicating a strong perpendicular magnetization is realized for the film with Ge underlayer (b) [106-108].

Magnetization structure observations were also carried out by employing high-resolution magnetization observation techniques such as Lorentz TEM [109], spin SEM [110], and magnetic force microscopy (MFM) [37, 75, 111-113]. MFM is the technique developed as an extension of scanning force microscopy invented in 1986 [114] and the technique started to be employed in the magnetics community from late 1980's. Since then, MFM has been most widely used to visualize the recorded information because of its easy operation and no special requirement of pre-processing for the observation samples. Figures 10 (a) and (b) compare the magnetization structure of PMR- and LMR-CoCrTa media with similar alloy

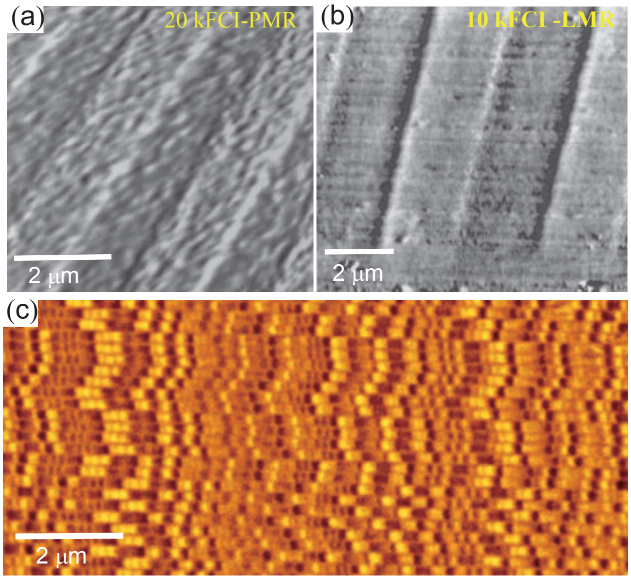

Fig. 10 MFM images of magnetization structure recorded on Co-alloy recording media, (a), (b): (1994, and (c) (2007) 2,113). (a) MFM image of Co-17at%Cr-5at%Ta perpendicular medium recorded at 20 kFCI. (b) MFM image of Co16at%Cr-4at%Ta longitudinal medium recorded at 10 kFCI. (c) MFM image of commercial PMR medium shipped in 2007 with an areal density of 185 Gb/in^2.

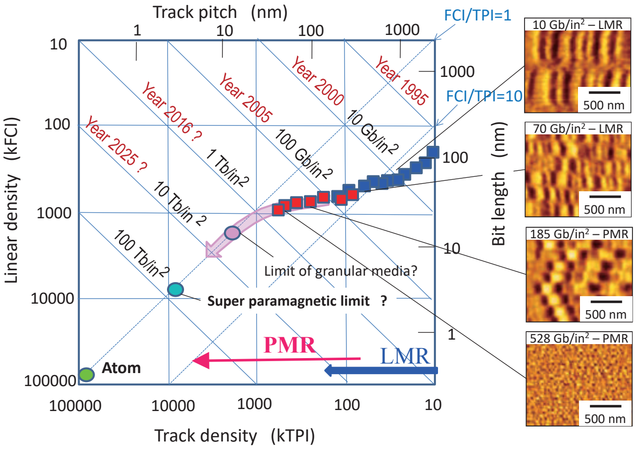

Fig. 11 Decreasing trend of bit size in commercial HDDs 2).

compositions observed in 1994 113). The LMR medium was observed with a relatively uniform MFM contrast within sharply recorded bit transitions, whereas the PMR medium was with an irregular MFM contrast and wavy bit transitions which correspond to higher medium noise and poorer recording resolution. The difference in magnetization structure was correlated with the nonmagnetic elements (Cr, Ta) segregation around the magnetic crystal grain boundaries, which was later confirmed to be depending on the crystal grain boundary structure. When deposited under a similar condition, enhanced segregation was achieved more easily with an LMR medium that included higher-angle crystal grain boundaries, whereas segregation of nonmagnetic elements was poor for a PMR medium consisting of *c*-axis oriented hcp-crystal grains which tended to form lower-angle crystal grain boundaries. The crystal lattice of *c*-axis oriented hcp-grain in PMR medium matches with that of neighboring crystal every 60 degrees of rotation along the perpendicular direction, whereas that of LMR medium with the *c*-axis lying in the film plane matches every 180 degrees and therefore crystal grains of LMR medium tend to form large angle crystal grain boundaries. Because the local stress in crystal grains of LMR medium presumably larger than that of PMR medium, Cr segregation was accelerated for the LMR medium.

The amorphous phase segregation along magnetic crystalline grain boundaries by employing SiO_x oxide as the nonmagnetic material sputter deposited together with a CoPt-alloy magnetic material, which was based on a two-phase separation mechanism, showed a drastic effect in forming very sharp compositional transitions from magnetic to nonmagnetic regions. As a result, smaller-size recorded bits surrounded by sharp magnetization transitions became possible as shown in the MFM image of CoCrPt-SiO_x perpendicular media depicted in Fig. 10 (c). The signal to noise ratio was improved and thus the continuous decrease in bit size became possible while keeping the thermal stability of recorded information which had caused problems with LMR media 7, 8). The decreasing trend of bit size in commercial HDDs is shown in Fig. 11 together with related MFM images 2). The bit shape is changing from an elongated rectangular to a square with increasing areal density and by shifting the recording technology from LMR to PMR.

With increasing areal density toward 1 Tb/in^2, the bit length is decreasing to be shorter than 25 - 30 nm where a spatial resolution of 10 nm or better is necessary to clearly observe the recorded bit patterns. Since the spatial resolution of commercially available MFM tip was limited at around 20 nm, the structure and the magnetic material for MFM tip fabrication were systematically investigated to improve the spatial resolution and the magnetic switching field 115-119). High magnetic switching field is required for an MFM tip in the magnetization structure observation of high coercivity medium, where the tip is exposed to a strong magnetic flux emanating from the sample that may change the tip magnetization. When the tip magnetization changes, the MFM contrast varies during an observation process. MFM tips with high magnetic switching fields were prepared by coating high K_u magnetic materials on nonmagnetic base tips 120-122). Through optimization of tip fabrication condition, MFM tips with spatial resolutions of 6 - 7 nm could be developed 123, 124). The switching field was increased to be higher than 2 kOe with maintaining high spatial resolutions of 10 nm or better 117, 125).

Figure 12 shows the magnetization structure of 500 -

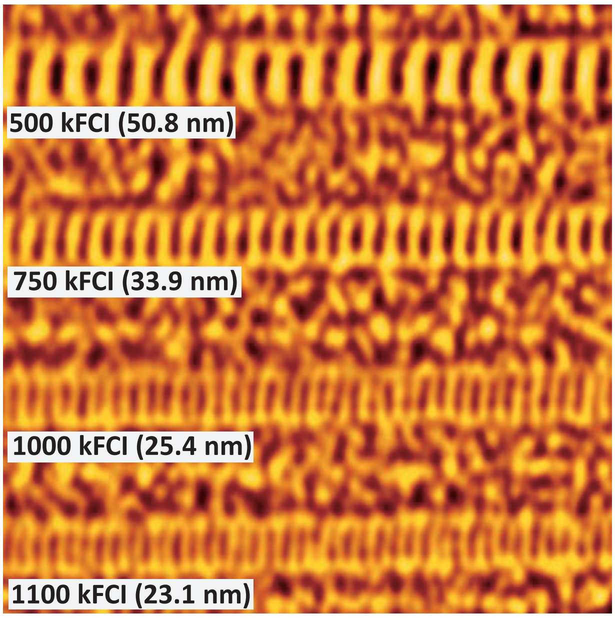

Fig. 12 Magnetization structure of 500 – 1100 kFCI (bit length: 50.8 – 23.1 nm) recording on a CoCrPt-SiO$_x$ PMR medium observed by using a high-resolution MFM tip, (2013) 118, 119).

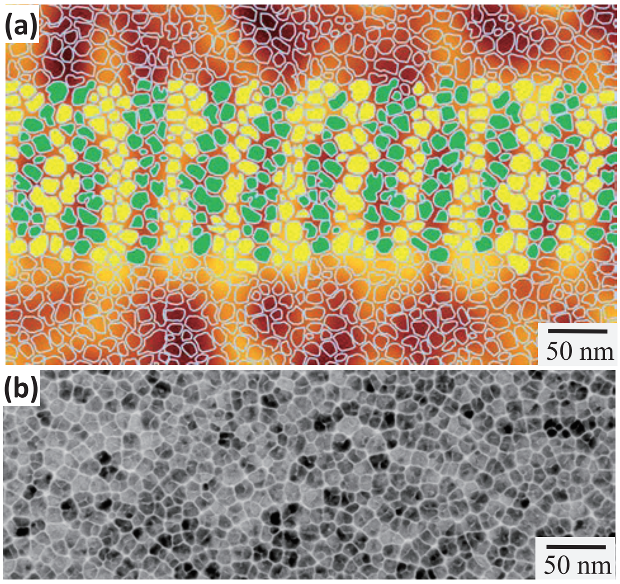

Fig. 13 Relationship between magnetization structure (1000 kFCI recording) and magnetic crystal grain distribution, (2013). The schematic MFM image, (a), is obtained by overlapping an MFM image with a plan-view TEM image, (b), observed for a same PMR medium 118,119).

1100 kFCI (bit length: 51 - 23 nm) recorded on a CoCrPt-SiO$_x$ PMR medium observed by employing a high-resolution tip 119). When a plan-view medium structure observed by TEM is overlapped with an MFM image, a relationship between the recorded magnetization and the magnetic crystal grain structures can be demonstrated as shown in Fig. 13 118). Here, the magnetic crystal grains along one track are colored for easy recognition of the inter-relationship. Although the two pictures (MFM and TEM images) were not observed for a same area but from different areas of a same medium sample, a detailed information how the individual bit is recorded on granular magnetic crystal grains can be revealed, which is useful in finding the points for further improving the medium structure to be more suitable for higher areal density magnetic recording 126).

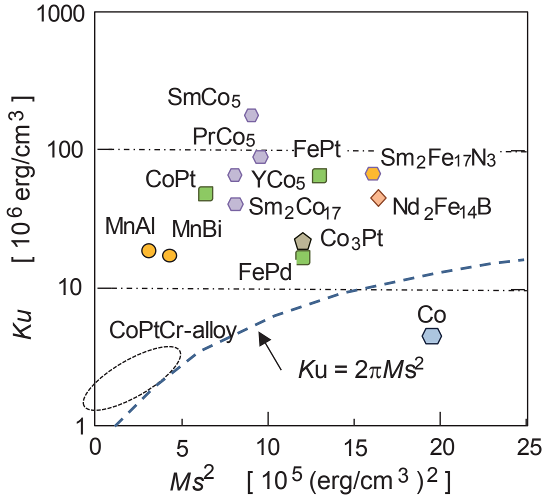

Fig. 14 K_u values of magnetic materials plotted as a function of $M_s{}^2$, 127-129).

6. Nanostructure tailoring of magnetic materials

6.1 High K_u magnetic materials

The K_u value of CoCrPt-alloy material used as the recording layer in the current HDDs is limited to be around 10^7 erg/cm^3 even the alloy composition and the media production process conditions are modified. Magnetic materials with higher K_u values are required for further increasing the recording density. The volume (V) of magnetic crystal grain included in a magnetic bit of recording layer needs to be continuously decreased while keeping the thermal stability condition of recorded information, $K_u V / k_B T$ > 35-70 127, 128), where k_B is Boltzmann's constant and T is absolute temperature. There are candidates for such magnetic materials with K_u values greater than 10^7 erg/cm^3; (1) magnetic multilayers of Co and noble metals, Co/Pd, Co/Pt, (2) ordered alloys of rare-earth and 3d-transition metals, $SmCo_5$, $PrCo_5$, $GdCo_5$, Sm_2Co_{17}, etc., (3) alloys of 3d-transition and noble metals with ordered structures, $L1_0$-FePt, $L1_0$-FePd, $L1_0$-CoPt, $D0_3$-Co_3Pt, τ-MnAl, (4) Co-Pt alloys with metastable ordered structures, $L1_1$-CoPt, B_h-CoPt, and (5) other compounds, $Nd_2Fe_{14}B$, $Sm_2Fe_{17}N_3$, α-MnBi, etc. Figure 14 shows the K_u values of magnetic materials plotted as a function of Ms^2, which are cited from the references127-129). For application to PMR media, the K_u should be larger than the magneto-static energy ($2\pi M_s{}^2$), thus a relation, $K_u > 2\pi M_s{}^2$, must be satisfied. The materials above the $K_u = 2\pi M_s{}^2$ line shown in Fig.

14 are basically applicable to PMR media. However, for practical applications, several conditions such as for aligning the easy magnetization axis perpendicular to the substrate, for achieving higher order degrees in ordered alloys to get high K_u values, for controlling the crystal grain size suitable for magnetic recording, chemical stability, etc. must be considered. These conditions are usually different depending on the material and thus must be investigated independently for the respective magnetic material. Some of the basic conditions in tailoring the crystal structure, the crystal orientation, the chemical ordering, etc., have been investigated by employing epitaxial magnetic thin films prepared on nonmagnetic single-crystal substrates. For example, it has been shown that the easy magnetization axis of $SmCo_5$ ordered alloy and related compounds of RT_5-type ordered structure (R: rare-earth element, T: 3d-transition element), YCo_5, $GdCo_5$, $SmNi_5$, $SmFe_5$, etc., which possess K_u values in the order 10^6 – 10^8 erg/cm^3, can be aligned perpendicular to the substrate by employing a Cu(111) 130-137) or a Ru(0001) underlayer 138). The effects of deposition temperature and film composition on the formation of ordered alloys and the degree of ordering are also investigated by using an UHV-MBE with co-evaporation of R and T elemental materials. Amorphous phases tend to be mixed with RT_5-ordered crystals when the composition shifts from the optimum ranges which depend delicately on the R-T material combination 130, 134). Substrate temperature higher than 500 °C is necessary for the preparation of RT_5-type epitaxial thin films on Cu(111) and Ru(0001) underlayers. Higher temperature, however, promotes diffusion of metallic Cu or Ru to the magnetic layer 131, 139), which generally lowers the K_u value. Further studies for forming a sharp interface while achieving a high order degree in the RT_5 structure in very thin films of less than 10 nm in thickness are apparently necessary for the application to future perpendicular recording media. Chemical stability of RT_5 material is an issue to be solved before practical applications, since rare-earth elements react easily with oxygen or water vapor.

6.2 Magnetic multilayer films

Magnetic multilayers of Co and noble-metal element (Pd or Pt) can be prepared at relatively low temperatures. From the investigations of Co/Pd multilayers deposited on single-crystal Pd underlayers of (001), (011), and (111) orientations at RT, it was shown that higher perpendicular magnetic anisotropies were observed for the epitaxial multilayer films prepared on fcc-Pd(111) underlayer 140, 141). The multilayer was composed of repeated number of stacked fcc-Co(111)/fcc-Pd(111) bi-layer with very thin Co-Pd alloyed regions at the Co/Pd interface 142-144). Perpendicular magnetic anisotropy increased with increasing the repetition number, and the origin was interpreted to be coming from an interface anisotropy and a magneto-crystalline anisotropy of Co-Pd(111) alloy-crystal whose lattice was slightly deformed along the perpendicular direction in accommodation of a large lattice misfit of 9.2% between the fcc-Co and the fcc-Pd layers 145). As no ordered phase exists in the Co-Pd binary phase diagram 146), the origin of perpendicular anisotropy is possibly due to a presence of very thin metastable structure similar to $L1_1$-phase which has a high K_u and is recognized in a CoPt alloy material 147).

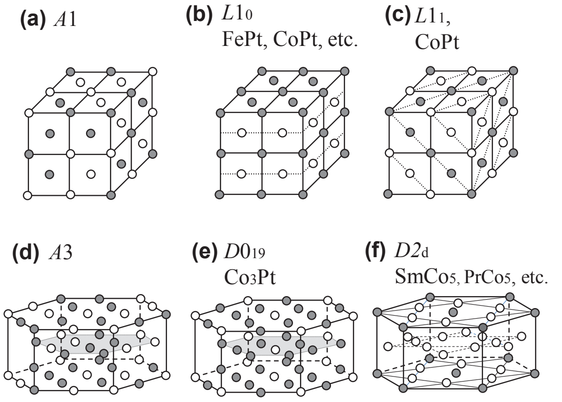

Fig. 15 Crystal structures of high K_u magnetic materials, based on fcc-cubic ($A1$) and hexagonal ($A3$) lattices.

The magnetic anisotropy and the saturation magnetization can be controlled in a certain range to be usable for magnetic recording media by varying the thickness ratio of the Co and Pd layers and the repetition number of Co/Pt bi-layer. Although a low substrate temperature for film formation and a high perpendicular magnetic anisotropy are the advantages with multilayer magnetic films, they are not easy to be tuned for application to granular-type perpendicular media. The multilayer films are considered to be more suitable for the bit patterned media which involve nanometer scale fabrications using chemical etching, ion-beam, or other sophisticated techniques 148-150).

6.3 Magnetic materials with ordered structures

The high K_u magnetic materials of (2) - (5) groups are with ordered structures consisting of more than two elements with atomic arrangements specific to the respective ordered structures. Figure 15 shows the typical crystal structures of high K_u magnetic materials. Table 2 lists the structural and magnetic properties of high K_u magnetic materials 127-129, 151-156). The degree of atomic ordering in a magnetic material, where a higher order degree corresponds to a higher K_u value, depends on the processing condition, in particular, the temperature. Thus higher substrate temperatures are generally necessary for film preparations. In these high K_u magnetic materials, the alloys of 3d-transition and noble metals with $L1_0$-type ordered structure, $L1_0$-FePt, $L1_0$-FePd, and $L1_0$-CoPt alloys, have been most intensively investigated for the granular-type recording layers 127, 128, 157-161). Thus, high K_u magnetic materials with $L1_0$ ordered structure are focused in the present

Table 2 Structure and magnetic properties of high K_u magnetic materials [127-129, 151-156].

Material	Crystal structure	K_1, (10^7 erg/cm^3)	M_s, (emu/cm^3)	T_c, (K)
$L1_0$ phases	Tetragonal (*fcc*-based)			
FePt	a = 384 pm, c = 370 pm, c/a = 0.96	6.6	1140	750
FePd	a = 381 pm, c = 372 pm, c/a = 0.98	1.8	1100	749
CoPt	a = 377 pm, c = 370 pm, c/a = 0.98	4.9	770	840
τ-MnAl	a = 392 pm, c = 357 pm, c/a = 0.91	1.7	560	650
$B8_1$ phase	Hexagonal			
α-MnBi	a = 428 pm, c = 611 pm, c/a = 1.43	1.2	700	633
$L1_1$ phase	CuPt-type rhombohedral (*fcc*-based)			
CoPt	a = 534 pm, α = 61.5°	3.7 (S = 0.54)	800	-
$D0_{19}$ phase	Rhombohedral (*hcp*-based)			
Co_3Pt	a = 367 pm	2.0	1100	1190
Compounds of rare-earth and transition elements	Hexagonal			
$SmCo_5$	a = 499 pm, c = 398 pm, c/a = 0.80	11 - 20	910	1020
YCo_5	a = 494 pm, c = 398 pm, c/a = 0.81	5 - 6.5	850	987
$PrCo_5$	a = 501 pm, c = 399 pm, c/a = 0.80	8.3	930	885
$GdCo_5$	a = 498 pm, c = 397 pm, c/a = 0.80	4.6	498	1014
Sm_2Co_{17}	a = 838 pm, c = 1221 pm, c/a = 1.45	4.2	838	1190
$Sm_2Fe_{17}N_3$	a = 873 pm, c = 1264 pm, c/a = 1.45	8.6	1230	749
	Tetragonal			
$Nd_2Fe_{14}B$	a = 879 pm, c = 1218 pm, c/a = 1.39	4.6	1270	588

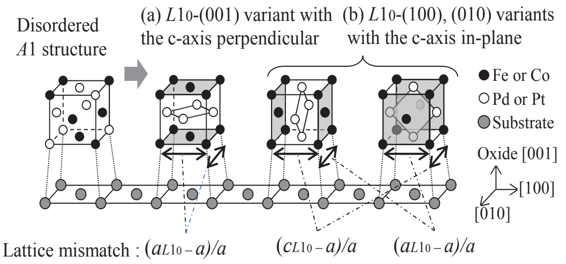

Fig. 16 Possibilities of phase transformation from disordered $A1$ structure to $L1_0$ ordered structure. The c-axis of $L1_0$(001) variant crystal is perpendicular to the substrate surface, whereas the c-axis is in-plane for the $L1_0$(100) and (010) variant crystals. The lattice mismatch is supposed to give an influence which type of variant crystal is likely favored.

review. Concerning the preparation and the characterization of other-type ordered alloy films of RT_5, $L1_1$-CoPt, B_h-CoPt, and $D0_{19}$-Co_3Pt, they are reported in the references [130-139, 162-172].

There are technical issues associated with the materials of $L1_0$ ordered structure to be solved for application to PMR recording media. They are basically similar to the case of conventional Co-alloy material with an hcp structure, but are more complicated. The technologies for aligning the easy magnetization axis of $L1_0$-magnetic-crystal grain perpendicular to the substrate surface and for preparation of a flat medium surface that can allow a very narrow spacing of less than a few-nm between the medium and a magnetic head. The latter is a newly added issue associated with the magnetic material which will be used for HDDs with the areal densities greater than 2 - 3 Tb/in^2, where a new-type media, bit patterned media (BPM), is included. Preparation of magnetic crystal with $L1_0$-ordered structure involves atomic ordering from a disordered fcc ($A1$ structure), which is different from the case of traditional Co-alloys. The possibilities of easy magnetization distribution associated with the phase transformation from $A1$ to $L1_0$ ordered structure are shown schematically in Fig. 16. Here, the underlayer of oxide with NaCl-type structure is assumed, considering that magnesium oxide (MgO: NaCl-type structure) has been widely used as an underlayer for aligning the easy magnetization axis (c-axis) perpendicular to the film plane. $A1$ structure based crystallographic notations for the direction and the plane are employed in this paper for the $L1_0$-ordered structure to make easy comparison with those of $A1$ structure, though the unit-cell of $L1_0$-ordered structure is tetragonal as shown in Table 2.

The easy magnetization axis of $L1_0$-orederd magnetic crystal is the c-axis. When an atomic ordering takes place in a bulk crystal of $A1$ structure, there are three possibilities of c-axis orientation with the ordered $L1_0$ structure, $L1_0$ [100], [010], and [001] parallel with respect to the original $A1$ [001], as shown in Fig. 16. Three kinds of $L1_0$ crystal domain variant with the c-axis perpendicular each other were observed in the high-resolution TEM pictures of FePt film samples prepared on NaCl(001) substrates [173, 174]. The presence of crystal domains with the c-axis lying in the film plane deteriorates the perpendicular magnetic anisotropy and widens the magnetic switching field distribution of media, both of which are undesirable for high density magnetic recording applications.

The other issue is the surface roughness of granular-type magnetic layer consisting of $L1_0$ ordered magnetic crystal grains. Possibly due to a large difference in surface energy between the magnetic material (FePt, FePd, or CoPt) and the oxide underlayers (MgO, etc) and to a high substrate temperature for enhancing $L1_0$ ordering, the magnetic material tends to form crystal grains of spherical or facetted shape with different diameters forming notable surface undulations, which may hinder a closer approach of magnetic head in performing a high density magnetic recording. Basic technologies in controlling the crystallographic orientation and in forming thin films with reduced surface undulations are briefly explained in the following sections.

(a) *c*-axis alignment of $L1_0$-ordered magnetic crystal

In order to apply $L1_0$-oredered alloy magnetic films to PMR media, the *c*-axis of crystal grain must be aligned perpendicular to the film surface. The alignment involves a more complicated technology compared with the case used for the conventional hcp-Co-alloy crystal. This is because that $L1_0$-crystal structure is based on cubic (*A*1, fcc) structure with three crystallographic symmetries compared with less crystallographic symmetries in the hcp-structure (*A*3). When a magnetic material is deposited on a substrate where an $L1_0$-ordered alloy crystal with the basal $L1_0$-(001) plane parallel to the surface is expected through an epitaxial growth mechanism, there are other possibilities of crystal growth with the $L1_0$-(100) and the $L1_0$-(010) planes parallel to the surface as well. This is due to that the atomic arrangement of $L1_0$-(001) is similar to that of other planes and the unit size of $L1_0$-(001) basal plane ($a \times a$) is very similar to that of other $L1_0$-(100) and $L1_0$-(010) planes ($a \times c$), where the c/a ratios of $L1_0$ crystals are very close to unity ranging between 0.96 and 0.98 for the ordered FePd, FePt, and CoPt materials as listed in Table 2. When the order degree decreases, the c/a ratio approaches to 1.0 [175] thus reducing the difference in lattice dimension between the $L1_0$-(001) basal plane and the other $L1_0$-(010), $L1_0$-(100) planes. As a result, three possibilities of ordering from disordered *A*1 structure to $L1_0$-ordered structure exist as shown schematically in Fig. 16.

Table 3 shows the distributions of $L1_0$-crystal variants which were investigated for FePd, FePt, and CoPt magnetic materials [153, 176]. 40 nm thick films were deposited on the single-crystal substrates of MgO, $SrTiO_3$, and $LaAlO_3$ with (001) orientation at a substrate temperature of 600 °C. The lattice constants of substrate material and the misfits with the magnetic materials are also shown in Table 3. All the magnetic films grew epitaxially on the (001) single-crystal substrates. The $L1_0$-variant configurations and order degrees were carefully investigated by reflection high-energy reflection diffraction (RHEED) and by X-ray diffraction (XRD) employing out-of-plane and in-plane measurements. Similar results on the variant configurations and the order degrees are confirmed for the magnetic materials of 40 nm thickness prepared by employing a two-step process which consists of low temperature deposition at 200 °C followed by high temperature annealing at 600 °C [153, 177]. When the magnetic materials were deposited at 200 °C, the films grew epitaxially with the disordered *A*1 structure. In the case of two-step process, an ordering from disordered *A*1 structure to $L1_0$-ordered structure is taking place during the annealing process at 600 °C. On the $LaAlO_3$(001) substrate, two-types of variant crystal were coexisting for the three magnetic materials. On the contrary, FePd film grew with the $L1_0$-(001) plane parallel to the substrate surface on the MgO(001) and the $SrTiO_3$(001) substrates and the $L1_0$-(100), (010) variants were not recognized. However, two variant crystals were coexisting on the $LaAlO_3$(001) substrate. FePt and CoPt films were consisting of two-types of variant crystal on these oxide substrates. The data indicate that $L1_0$-crystal variant structure changes depending on the combination of magnetic and substrate materials. It also shows that the order degree, S, is different between the $L1_0$-variant crystals with the *c*-axis perpendicular and in-plane for a magnetic film. Higher order degrees tend to be observed for the $L1_0$-(001) variants than for the $L1_0$-(100) + (010) variants as shown in the cases of CoPt on MgO, $SrTiO_3$, and $LaAlO_3$ substrates, FePt on $SrTiO_3$ and $LaAlO_3$ substrates, and FePd on $LaAlO_3$ substrate. Such difference seems to be caused by a delicate difference of atomic movement within a magnetic crystal during the ordering process, which is possibly related with the internal stress of magnetic crystal caused by a lattice misfit with the substrate lattice.

Higher S value of $L1_0$-(001) variant is observed in the order FePd > FePt > CoPt on the oxide substrates, indicating that the activation energy for $L1_0$-ordering is the lowest for the FePd material. When the order degree is compared for the FePd films deposited on MgO, $SrTiO_3$, and $LaAlO_3$ substrates, higher S value is observed in the order MgO > $SrTiO_3$ > $LaAlO_3$. This tendency is similar to the order of lattice misfit, $(a_{L10} - a)/a$, where a_{L10} is the lattice length of $L1_0$-(001) basal plane and a is the lattice constant of oxide crystal. A negative larger lattice misfit along $L1_0$ [100], [010] can be interpreted to yield a higher S value in the $L1_0$-(001) variant. The rule is also applicable for the S value of $L1_0$-(001) variant in CoPt film. The data for FePt film show almost similar tendency but with a reversed order between the $LaAlO_3$ substrate ($S = 0.30$, misfit = - 0.8%) and the $SrTiO_3$ substrate ($S = 0.34$, misfit = - 0.2%). The discrepancy may be within an experimental error since the misfit difference is only 0.6%. The stress in $L1_0$-(001) variant crystal caused by a lattice misfit with the substrate is considered to have given a positive effect in enhancing ordering.

Table 3 shows that the ratio of $L1_0$-variants with the *c*-axis perpendicular and in-plane differs depending on

Table 3 $L1_0$ crystal variants in magnetic thin films deposited on different oxide substrates[153, 176].

Substrate	Property	Magnetic material		
		FePd a_{L1_0} = 381 pm, c_{L1_0} = 372 pm	FePt a_{L1_0} = 384 pm, c_{L1_0} = 370 pm	CoPt a_{L1_0} = 377 pm, c_{L1_0} = 370 pm
MgO (001) a = 421 pm	V_{L1_0} (001)	100 %	35 %	41 %
	S_{L1_0} (001)	0.69	0.34	0.23
	$(a_{L1_0} - a)/a$	- 9.7 %	- 8.7 %	- 10.0 %
	V_{L1_0} (100), (010)	0 %	65 %	59 %
	S_{L1_0} (100), (010)	-	0.39	0.03
	$(c_{L1_0} - a)/a$	-11.8 %	-12.1 %	-12.1 %
$SrTiO_3$ (001) a = 390 pm	V_{L1_0} (001)	100 %	40 %	48 %
	S_{L1_0} (001)	0.61	0.38	0.20
	$(a_{L1_0} - a)/a$	- 2.6 %	- 1.6 %	- 3.3 %
	V_{L1_0} (100), (010)	0 %	60 %	52 %
	S_{L1_0} (100), (010)	-	0.33	0.06
	$(c_{L1_0} - a)/a$	- 4.9 %	- 5.2 %	- 5.1 %
$LaAlO_3$ (001) a = 381 pm	V_{L1_0} (001)	42 %	42 %	40 %
	S_{L1_0} (001)	0.51	0.30	0.15
	$(a_{L1_0} - a)/a$	- 0.2 %	+ 0.8 %	- 1.0 %
	V_{L1_0} (100), (010)	58 %	58 %	60 %
	S_{L1_0} (100), (010)	0.19	0.22	0.11
	$(c_{L1_0} - a)/a$	- 2.5 %	- 2.9 %	- 2.9 %

V_{L10} (001): volume ratio of variant with c-axis perpendicular to the substrate. S_{L10} (001): order degree of $L10$ (001) variants.
$(aL10 - a)/a$: lattice mismatch between $L10$-crystal and the substrate.
V_{L10} (100) + (010) : volume ratio of variants with c-axes in-plane. S_{L10} (100) + (010) : order degree of $L10$ (100) + (010) variants.
$(cL10 - a)/a$: lattice mismatch between $L10$ (100) or (010) crystal and the substrate.

the combination of magnetic material and substrate. Considering the volume ratio (33%) of $L1_0$-(001) variant expected when the phase transformation from $A1$ to $L1_0$ structure is taking place randomly, the nucleation of $L1_0$-(001) variant is apparently favored since the volume ratio exceeds 33% for all the combinations. However, it is not easy to discern which factor is playing a dominant role in fixing the variant orientation. Only the $L1_0$-(001) variant is observed for the FePd films formed on MgO and $SrTiO_3$ substrates, but on $LaAlO_3$ substrate two kinds of variant are coexisting. For FePd film, a larger negative lattice misfit with the substrate seems to be working to promote the nucleation of $L1_0$-(001) variant. However, this rule is not straightforwardly applicable to the FePt and the CoPt cases. Some other material factors such as activation energy of atomic diffusion in magnetic crystal, $L1_0$ crystal nucleation density, and mechanical property like Young's modulus are considered to be working in addition to the lattice misfit effect.

The variant configurations were investigated for the 40 nm-thick $Fe_{50}(Pt_{1-x}Pd_x)$ alloy films deposited on MgO(001) substrate to study the influence of Pd to Pt ratio on $L1_0$ variant structure[178, 179]. The result showed that the films with $x > 0.5$ consisted of $L1_0$(001) crystals, whereas the films with $x < 0.25$ included $L1_0$(100) crystals with the c-axis lying in the film plane. Such data is apparently indicating that material related factors are giving influences in fixing the $L1_0$-variant crystal orientation. The effect of strain caused by lattice misfit on $L1_0$ variant configuration can be investigated by employing film samples with different thicknesses, since the tension force caused by a misfit between the substrate and the deposited magnetic material decreases with increasing the magnetic layer thickness along the film growth direction. The effects of magnetic layer thickness on the variant structure and the order degree were investigated for FePd films deposited on MgO(001) substrates [180]. Although the films thinner than 40 nm consisted of $L1_0$(001) crystal, a notable volume of $L1_0$(100) and $L1_0$(010) variants started to be included when the film thickness was increased to be larger than 100 nm. The easy magnetization axis varied from perpendicular to in-plane, as the thickness was increased from 100 to 500 nm where the volume percentage of $L1_0$(001) variant decreased down to about 20% which is lower than that expected for random nucleation (33%). The order degree of $L1_0$ structure also decreased with increasing the magnetic layer thickness. Similar data were obtained for FePt thin films [181]. These results show that the lattice strain caused by misfit with the substrate material is playing an important role in fixing the $L1_0$ variant configuration and in enhancing the ordering degree.

The effects of variant configuration and the order degree are also investigated for magnetic materials formed on fcc (001) metallic underlayers such as Ag, Au, Pt, Pd metals epitaxially grown on MgO(001) substrates [182]. Although 10 nm thick FePt films deposited at a substrate temperature of 600 °C grew with the c-axis of $L1_0$ structure perpendicular to the substrate surface they included $L1_0$(100) variants. The order degree varied widely in a range between 0.2 – 0.78 depending on the fcc underlayer material, which is different from the cases of oxide substrate. The difference may be attributed to the difference of lattice strain in the magnetic material around the interface between the metallic underlayer and the oxide substrate. In the cases of metallic underlayer, the strain will be more easily relaxed due to similar Young's modulus and possibly due to element's

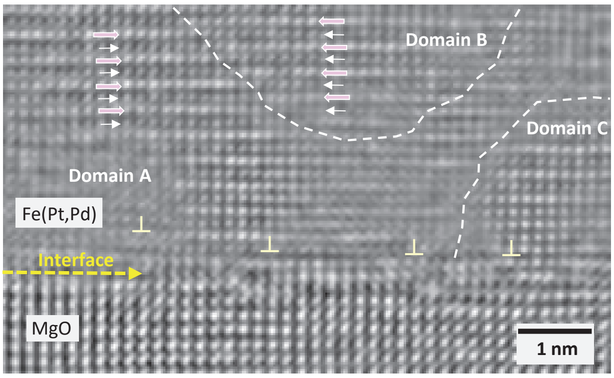

Fig. 17 High-resolution TEM image of interface between MgO(001) substrate and $L1_0$-ordered Fe(Pt, Pd) epitaxial thin film. The thick and thin arrows respectively show the lines enriched with high atomic number atoms (Pt, Pd) and with low atomic number atoms (Fe) corresponding to the atomic stacking along [001] of $L1_0$-ordered structure. The dotted lines show the anti-phase boundaries and the mark $\perp$ shows the misfit dislocation [181].

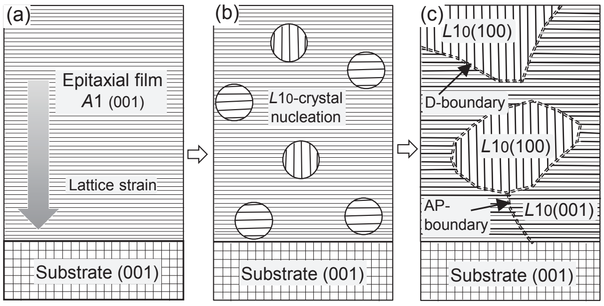

Fig. 18 Schematic model to explain the nucleation and growth of $L1_0$-crystal variants in disordered $A1$ phase matrix. (a) Lattice of $A1$ crystal epitaxially grown on MgO(001) substrate is strained to accommodate the lattice mismatch, where the $A1$ lattice is expanded in lateral direction whereas it is contracted in vertical direction. (b) Nucleation of $L1_0$-crystal is influenced by the $A1$ lattice strain. $L1_0$(001) crystal with $c/a < 1$ will be formed preferentially in a region close to the substrate interface while a more isotropic nucleation will take place in a region away from the interface. (c) Coalescence of growing crystal variants forms domain boundaries (D-boundary). Neighboring $L1_0$(001) crystals with a half-pitch difference (d_{002}) in the atomic stacking forms an anti-phase boundary (AP-boundary) [181].

diffusion across the interface of the two layers. These experimental results indicate that the lattice misfit of magnetic material with respect to the substrate, the underlayer, or the interlayer plays important roles in determining the variant orientation as well as the degree of $L1_0$ ordering.

The structure variation from $A1$ to $L1_0$ phase was investigated by XRD and HRTEM observations for FePt and FePd films on MgO(001) substrates as a function of film thickness to study the $L1_0$ variant crystal growth mechanism [181]. The results indicate that the resulting $L1_0$-variant structures are related with the degree of lateral lattice strain existing in the $A1$ phase film and that the preferential formation of $L1_0$(001) variant is due to larger lattice strains in the FePd film compared with the case of FePt film.

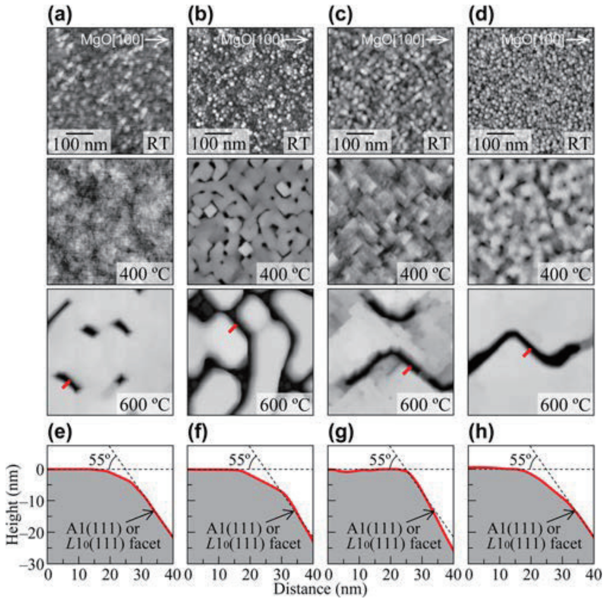

Fig. 19 AFM images of (a) FePt, (b) FePd, (c) CoPt, and (d) CoPd films grown at different substrate temperatures.
(e)–(h) Cross-sectional profiles along the red lines in (a)–(d), respectively [185].

The effects of lateral lattice strain on $L1_0$-ordering were also studied for 10-nm-thick FePt films deposited on (001) oriented oxide single crystal substrates of MgO, $MgAl_2O_4$, $SrTiO_3$, and $LaAlO_3$ at a low substrate temperature of 200 °C and then annealed at 600 ° C [183], where the lattice mismatch of $A1$-FePt crystal with respect to the substrate ranged from -9.8% to +1.0%. Higher $L1_0$-ordering degree, S, is observed as MgO > $MgAl_2O_4$ > $SrTiO_3$ > $LaAlO_3$. The XRD and HRTEM study has shown that the lattice strain existing in the disordered ($A1$) film decreases during the high temperature $L1_0$-ordering process through introduction of misfit dislocations. The net misfit between $L1_0$-crystal and MgO(001) substrate is estimated to be less than 0.5% for the $L1_0$-ordered film. Figure 17 is an example of interface structure of $L1_0$-ordered Fe(Pt,Pd) epitaxial film formed on MgO(001) substrate. From the distributions of variant domain boundaries observed by HRTEM, the variant size is estimated to be 2 - 5 nm in diameter. A nucleation and growth model for explaining the $L1_0$-variant structure formation mechanism shown in Fig. 18 suggests a possibility in tailoring the variant structure in $L1_0$-ordered magnetic thin films by controlling the alloy composition, the layer structure, and the substrate material.

(b) Reduction of surface roughness for $L1_0$-ordered magnetic thin films

When a magnetic material is deposited on a substrate, atom migration, adhesion to the substrate surface, and formation of three-dimensional clusters take place. The film growth mode depends basically on a difference between the binding energy of deposited atoms, E_f, and the energy to bond to the substrate, E_{fs}. In a case $E_{fs} > E_f$, the film growth takes place with the Frank-van der Merwe growth mode or the layer by layer mode, whereas the film growth follows the Volmer-Weber growth mode or the island-type growth mode for $E_{fs} < E_f$ 184). Most of the combinations of magnetic materials (FePt, FePd, CoPt) and oxide substrates belong to the latter case. However, as the migration and diffusion behaviors of deposited atoms are influenced by the film formation process such as the deposition method and the substrate temperature, the resulting film nanostructure varies depending on these conditions, primarily on the substrate temperature. Figure 19 shows the variation of surface profiles observed for 40 nm-thick FePt, FePd, CoPt, and CoPd films deposited on MgO(001) substrates at RT, 400 °C, and 600 °C. Epitaxial growth is realized for all the films 185). The nm-scale film surface undulations are caused by the atomic movements reflecting the surface energy variations of crystal facet as schematically illustrated in Fig. 19 (e)-(h). When the substrate temperature is lower than 200 °C, the films are continuous with relatively smooth surfaces. The arithmetical mean surface roughness, R_a, values for these films are less than 2 nm. However, with increasing the substrate temperature, the surface roughness increases to be larger than 10 nm and deep crevices are observed for the $L1_0$ ordered films prepared at 600 °C, which are caused by clustering of deposited magnetic material and consisting of facetted surfaces. Surface roughness caused by clustering at elevated substrate temperatures is noted for the $L1_0$-(001) oriented polycrystalline thin film media 186-188).

Considering that the film morphology is influenced during the film deposition process, a two-step process technique consisting of a low temperature film deposition followed by a high temperature annealing for $L1_0$ ordering has been investigated to prepare an $L1_0$ ordered film with improved surface flatness 153, 174, 175, 177). Figure 20 compares the surface structures of FePd thin films of 2 - 40 nm thicknesses observed by atomic force microscopy (AFM). The films were deposited on MgO(001) substrates at 200 °C and then annealed at 600 °C. Smooth and continuous surface structures are realized for the films with thickness larger than 5 nm, showing an effectiveness of the two-step technique for the preparation of flat thin films. The surface roughness R_a of 40 nm-thick film prepared by employing the technique is as small as 0.15 - 0.3 nm. On the contrary, isolated island-like cluster structures are observed for the films thinner than 2 nm, where a clustering force of Fe and Pd atoms has apparently overcome the lateral binding force in the film. The degrees of $L1_0$ ordering in the films prepared by using the two-step method are similar to those of films directly deposited at 600 °C 180).

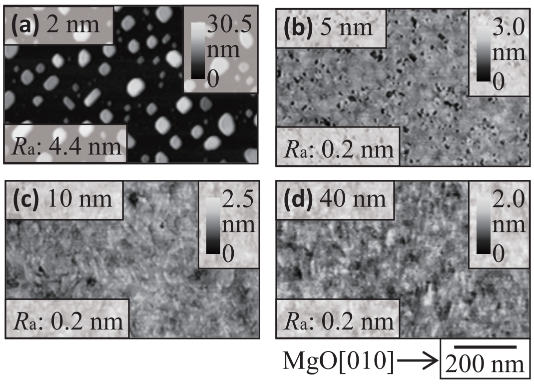

Fig. 20 AFM images of $L1_0$ ordered FePd films with (a) 2, (b) 5, (c) 10, and (d) 40 nm thicknesses prepared on MgO (001) substrates by deposition at 200 °C followed by annealing at 600 °C 175).

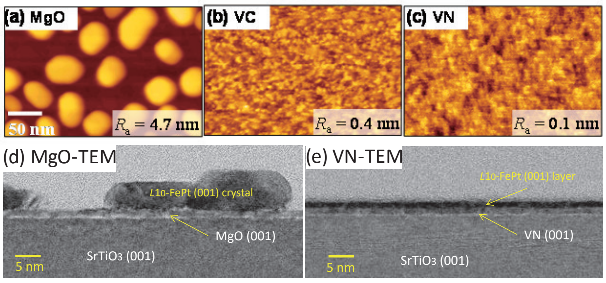

Fig. 21 AFM images of $L1_0$-FePt thin films of 2 nm in average thickness formed on (a) MgO, (b) VC, and (c) VN epitaxial underlayers 189). (d) Cross-sectional TEM image of $L1_0$-FePt film of 2-nm average thickness formed on MgO layer and (e) cross-sectional TEM of 2-nm thick $L1_0$-FePt film formed on VN epitaxial layer. (a) (d) and (c) (e) images are for the same samples, respectively.

Although the two-step method is useful for the preparation of $L1_0$-ordered thin film with a flat and continuous surface down to a thickness around several nanometers, island-like isolated crystals are formed when the thickness is further decreased. In order to prepare a continuous thin film, the energy balance working on an isolated island needs to be considered. As a deposited material behaves like a liquid droplet on the substrate surface at high temperatures, the contact angle of island to the substrate surface is determined by a balance working between the surface energies of substrate (γ_{SG}), deposited material (γ_{LG}), and interfacial energy between these materials (γ_{SL}), which is known as Young relationship 189). For achieving a lower contact angle, the condition, $\gamma_{SG} > \gamma_{SL} + \gamma_{LG}$, must be satisfied. Thus it seems useful to employ a substrate material of which surface energy is larger than that of magnetic material (FePt, FePd, CoPt). Figure 21 compares the morphology of $L1_0$-FePt(001) films of 2 nm average thickness formed on MgO (γ_{SG} = 1.4 J/m^2), VC (2.8 J/m^2), and VN (2-3 J/m^2) single-crystal underlayers of (001) orientation by employing the two-step method 190). The

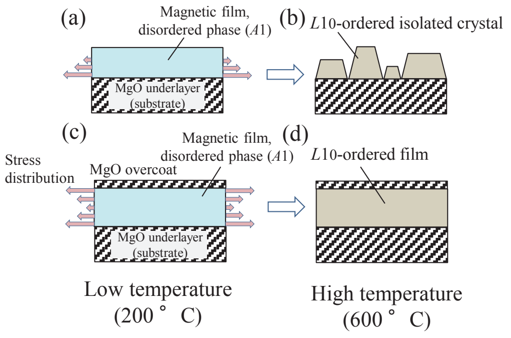

Fig. 22 Schematic model of $L1_0$ ordering from disordered structure, $A1$, magnetic film without overcoat (a), (b) and with overcoat (c), (d) epitaxially grown on MgO(001) substrate at low temperature (200 °C) followed by high temperature annealing (600 °C). The overcoat prevents clustering of magnetic material during the annealing process, thus providing a smooth surface of $L1_0$-ordered film. The order degree, S, is higher for the film with overcoat than that without overcoat [190, 191]

underlayer materials have a common NaCl-type crystal structure with similar lattice constants of 0.41 - 0.42 nm and $L1_0$-FePt crystal grows epitaxially with the c-axis perpendicular to the substrate surface. Very flat and continuous films with the surface roughness, $R_a < 0.4$ nm, are formed on the VC and VN underlayers, whereas isolated $L1_0$-FePt islands are formed on the MgO underlayer ($R_a = 4.2$ nm). An employment of underlayer material which has a surface energy larger than that of magnetic material seems to be crucial for the preparation of $L1_0$-ordered continuous magnetic thin films with very flat surfaces.

An another possibility to prepare $L1_0$(001) oriented magnetic thin films with flat surfaces is an employment of a thin overcoat on top of the magnetic thin film prepared by using the two-step method [191, 192]. A thin overcoat, 2 nm thick MgO layer was formed at 200 °C on FePt/MgO(001) samples with different FePt film thicknesses before annealing at 600 °C. Very flat and continuous surfaces with the R_a values less than 0.5 nm were realized for the 1-10 nm thick $L1_0$(001) FePt epitaxial thin films. Here the overcoat is interpreted to have worked in suppressing the atomic movements in the surface region of magnetic film during the high temperature ordering process at 600 °C preventing a formation of clusters. Furthermore, higher order degrees are also observed for the magnetic films with the MgO overcoats compared with the values of films of same thickness without overcoats. Formation of MgO overcoat layer is effective also in enhancing $L1_0$ ordering providing a lateral tension force to the magnetic layer from the surface side. Figure 22 shows a schematic model explaining the effect of overcoat. The basic findings obtained from the experimental studies employing $L1_0$ epitaxial thin films are believed to be useful in tailoring the high K_u $L1_0$ magnetic thin films to be applied for practical recording media.

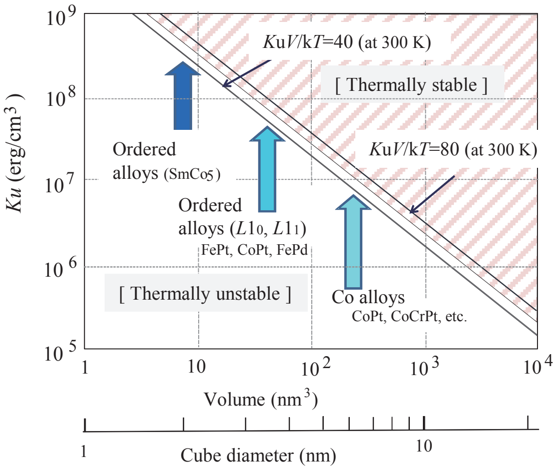

Fig. 23 Relationship between K_u and magnetic crystal grain volume for keeping the thermal stability condition, $K_uV/k_BT > 40 - 80$[126].

7. Future possibilities of high K_u magnetic materials

In order to apply the high K_u magnetic materials with $L1_0$ ordered structure for PMR media, practical technologies in tuning the nanostructure such as magnetic crystal grain isolation, high $L1_0$ ordering within a small crystal grain, appropriate control of grain size, narrow distribution of grain size, etc. while adjusting the magnetic properties, need to be developed. In addition, surface flatness and mechanical durability conditions that are related with very narrow physical spacing of less than a few nanometers between a magnetic head and a medium must be simultaneously satisfied. The development of such a highly sophisticated technology is a big challenge. However, the authors believe it will be possible likewise the past developments of media technology that enabled a dramatic areal density growth of HDD through intensive experiments carried out based on the basic science of materials.

Thermal stability of recorded information depends on $K_u V/k_B T$. When T is room temperature (300 K), the relation between magnetic crystal grain volume V (nm^3) and K_u (erg/cm^3) for maintaining the thermal stability is plotted as shown in Fig. 23 [2, 126]. Assuming the magnetic grain to be a cube shape, the cube edge length is also indicated as a measure in the figure. To decrease the length while keeping the thermal stability $K_u V/k_B T > 60$, K_u must be increased from the order of 10^6 erg/cm^3 which is with the Co-alloy materials currently employed as PMR media, to the order of 10^7 erg/cm^3 or higher. Although there are more than several magnetic materials with the K_u values higher than 10^7 erg/cm^3 as explained before, $L1_0$-ordered magnetic alloy materials seem to be the practical candidate for future PMR media because of the excellent chemical stability and the higher potential in tuning the nanometer level structure. The minimum edge length of cube crystal for keeping the thermal stability is calculated to be 3.4 nm for the $L1_0$-ordered FePt material which possesses the K_u value 6.6 × 10^7 erg/cm^3 129). Assuming a physical separation of 0.5 nm between magnetic crystals, the areal density will be increased up to around 40 Tb/in^2. If a $\mathrm{SmCo_5}$ crystal with the K_u value of 2 × 10^8 erg/cm^3 is applied, an areal density of more than 80 Tb/in^2 seems feasible. From thermal stability and available magnetic material points of view, an areal density of 100 Tb/in^2 which is more than 100 times larger than that of current areal density seems to be achievable by carefully tuning the sub-nanometer level structure of high K_u magnetic materials.

8. Summary

The developments of perpendicular magnetic recording media technology are briefly reviewed from a view point in tailoring the nanostructure of recording layer. Before establishing the PMR media structure that employs the granular-type Co-alloy recording layer with an hcp structure, there was a long history of research and development (R&D) since the invention of PMR in 1976. Including the early stage of R&D of Co-alloy recording layer, the technological developments in aligning the easy magnetization axis by hetero-epitaxial thin film growth and in achieving magnetic separation between the magnetic crystal grains by nonmagnetic elements segregation around the grain boundaries are explained. It is also shown that observations of composition and magnetization structures have played key roles for the improvement of medium nanostructure to be tuned suitable for high density magnetic recording.

Although Co-alloy recording layer materials have been used since the invention of PMR and will be continuously used up to an areal density beyond 1 Tb/in^2 by adding further tunings to the medium structure and possibly through a technological modification in the recording scheme 21, 22, 161), an employment of high K_u magnetic material is necessary for the recording layer in keeping the thermal stability of recorded information for further increasing the areal density well beyond 2 - 3 Tb/in^2. However, an employment of high K_u magnetic material brings in new technological issues which are different from those associated with conventional Co-alloy materials. From such viewpoints, basic research results related with technologies in controlling the easy magnetization and in keeping the surface flatness for $L1_0$-ordered magnetic thin films are also briefly explained. Finally, future possibilities of PMR media materials are discussed from the thermal stability of recorded information and the available magnetic material points of view. The authors believe that an areal density of 100 Tb/in^2 which is more than 100 times larger than that of current areal density seems to be achievable by carefully tuning the sub-nanometer level structure of magnetic materials.

Acknowledgements

The author (M. F.) would like to thank the colleagues at Hitachi CRL who worked with the author during "the dip period" lasted for 10 - 15 years, and the members of the committee 144 of the Japan Society for the Promotion of Science who worked toward the realization of PMR-HDDs, of which names are listed as the reference paper authors. The authors also thank the students of Chuo University who patiently collected valuable scientific data.

References

1) S. Iwasaki and Y. Nakamura: *IEEE Trans. Magn.*, **MAG-13**, 1272 (1977).
2) M. Futamoto: *IEICE Technical Report*, **MR2014-5**, 25 (2014).
3) Y. Uesaka, M. Koizumi, N. Tsumita, O. Kitakami, and H. Fujiwara: *J. Appl. Phys.,* **57** (1985) 3925.
4) W. Cain, A. Payne, M. Baldwinson, and R. Hempstead: *IEEE Trans. Magn.,* **32**, 97 (1996).
5) M. Oshiki: J. Mag. Soc. Japan., **21**, suppl. S1, 91 (1996).
6) D. A. Thompson: *J. Mag. Soc. Japan*, **21**, Suppl. S2, 9 (1997).
7) P-L. Lu and S. H. Charap: *IEEE Trans. Magn.*, **30**, 4230 (1994).
8) Y. Hosoe, I. Tamai, K. Takahashi, Y. Tanahashi, T. Yamamoto, T. Kanbe, and Y. Yajima: *IEEE Trans. Magn.,* **33**, 3028 (1997).
9) M. Futamoto, Y. Hirayama, N. Inaba, Y. Honda, K. Ito, A. Kikukawa, and T. Takeuchi: *IEEE Trans. Magn.* **35**, 2802 (1999).
10) H. Takano, Y. Nishida, M. Futamoto, H. Aoi, and Y. Nakamura: *Abstract of Intermag 2000*, AD-06.
11) T. Ando and T. Nishikawa: *IEEE Trans. Magn.,* **33**, 2983 (1997).
12) M. Futamoto, Y. Hirayama, Y. Honda, A. Kikukawa, K. Tanahashi, and A. Ishikawa: *J. Mag. Mag. Mater.*, **235**, 281 (2001).
13) K. Tanahashi, N. Shimizu, A. Kikukawa, Y. Honda, A. Ishikawa, and M. Futamoto: *J. Mag. Mag. Mater.*, **235**, 59 (2001).
14) Y. Kawato, M. Futamoto, and K. Nakamoto: *U. S. Patent*, US2002/0 028356A1 (2002).
15) M. J. Carey, Y. Ikeda, S. Smith, and K. Takano: *U.S. Patent* US2003/0 022 023 A1 (2003).
16) S. C. Byeon, A. Misra, and W. D. Doyle: *IEEE Trans. Magn.*, **40**, 2386 (2004).
17) S. Oikawa, A. Takeo, T. Hikosaka, and Y. Tanaka: *IEEE Trans. Magn.*, **36**, 2393 (2000).
18) Y. Tanaka and T. Hikosaka: *J. Mag. Mag. Mater.*, **235**, 253 (2001).
19) http://www.toshiba.co.jp/about/press/2004_12/pr1401.htm
20) Y. Tanaka: *Proc. IEEE*, **96**, 1754 (2008).
21) Y. Shiroishi, K. Fukuda, I. Tagawa, H. Iwasaki, S. Takenori, H. Tanaka, H. Mutoh, and N. Yoshikawa: *IEEE Trans. Magn.*, **45**, 3816 (2009).
22) A. Kikitsu, T. Maeda, H. Hieda, R. Yamamoto, N. Kihara, and Y. Kamata: *IEEE Trans. Mag.*, **49**, 693 (2013).
23) S. Iwasaki and K. Ouchi: *IEEE Trans. Magn.*, **MAG-14**, 849 (1978).
24) M. Futamoto, Y. Honda, and H. Kakibayashi: *Japan. J. Appl. Phys.*, **24**, L460 (1985).
25) Y. Honda, M. Futamoto, K. Yoshida, Y. Uesaka, Y. Shiroishi, and H. Kakibayashi: *IEICE Trans.*, **J69-C**, 85 (1986).
26) Y. Honda, M. Futamoto, S. Saito, and K. Yoshida: *IEICE Trans.*, **73-C11**, 74 (1990).
27) H. S. Gill and T. Yamashita: *IEEE Trans. Magn.*, **MAG-20**, 776 (1984).
28) R. Sugita, K. Takahashi, K. Honda, K. Kanai, and F.

Kobayashi: *Digests of the 6th Annual Conference of Magnetics in Japan*, pp.42 (1982).
29) H. S. Gill and M. P. Rosenblum: *IEEE Trans. Magn.*, **MAG-19**, 1644 (1983).
30) M. Futamoto, H. Honda, H. Kakibayashi, and K. Yoshida: *IEEE Trans. Magn.*, **MAG-21**, 1426 (1985).
31) P. W. Jong, Y. H. Kim, T. D. Lee, and T. Kang: *IEEE Trans. Magn.*, **25**, 4168 (1989).
32) Y. Hirayama and M. Futamoto: *J. Mag. Soc. Japan*, **19**, Suppl. No. S2, 14 (1995).
33) K. H. Krishnan, T. Takeuchi, Y. Hirayama, and M. Futamoto: *IEEE Trans. Magn.*, **30**, 5115 (1991).
34) D. J. Mapps, G. Pan, and M. H. Akhter: *IEEE Trans. Magn.*, **27**, 4168 (1991).
35) X. Song, J. Loven, J. Sivertsen, and J. Judy: *IEEE Trans. Magn.*, **32**, 3840 (1996).
36) M. Futamoto, Y. Honda, and K. Yoshida: *Journal de physique,* **Colloque C8**, Suppl. 12, Tome 49, C8-1979 (1988).
37) Y. Matsuda, M. Suzuki, Y. Hirayama, and M. Futamoto: *J. Mag. Soc. Japan*, **18**, suppl. No. S1, 99 (1994).
38) Y. Hirayama, M. Futamoto, K. Ito, Y. Honda, and Y. Maruyama: *IEEE Trans. Magn.*, **33**, 996 (1997).
39) A. Sato, S. Nakagawa, and M. Naoe: *IEEE Trans. Magn.*, **36**, 2387 (2000).
40) J. Ariake, N. Honda, K. Ouchi, and S. Iwasaki: *J. Mag. Mag. Mater.*, **242-245**, 311 (2002).
41) M. Futamoto, Y. Hirayama, N. Inaba, Y. Honda, ans A. Kikukawa: *IEICE Trans.*, **E84-C**, 1132 (2001).
42) M. Zheng, G. Choe, K. E. Johnson, L. Gao, and S-H. Liou: *IEEE Trans. Magn.*, **38**, 3193 (2002).
43) W. K. Shen, A. Das, M. Racine, R. Cheng, J. H. Judy, and J-P. Wang: *IEEE Trans. Magn.*, **42**, 2945 (2006).
44) U. Kwon, R. Sinclair, E. M. T. Velu, S. Malhotra, and G. Bertero: *IEEE Trans. Magn.*, **41**, 3193 (2005).
45) M. Futamoto, Y. Hirayama, Y. Honda, K. Ito, and K. Yoshida: *J. Mag. Soc. Japan*, **21**, Suppl. No. S2, 141 (1997).
46) Y. Hirayama, A. Kikukawa, Y. Honda, N. Shimizu, and M. Futamoto: *IEEE Trans. Magn.*, **36**, 2396 (2000).
47) M. Futamoto, Y. Hirayama, Y. Honda, and N. Inaba: *J. Mag. Mag. Mater.*, **226-230**, 1610 (2001).
48) M. Futamoto: *J. Optoelectron. Adv. Mater.*, **8**, 1861 (2006).
49) M. Futamoto, K. Terayama, K. Sato, and Y. Hirayama: *IEICE, Trans. Electron.*, **E85-C**, 1733 (2002).
50) M. Futamoto, K. Terayama, K. Sato, and Y. Hirayama: *Scr. Mater.*, **42**, 929 (2003).
51)W. Sucksmith and J. E. Thompson: Proc. *Roy. Soc. London*, Ser. A, **225**, 362 (1954).
52) Y. Takahashi, K. Tanahashi, and Y. Hosoe: J. Appl. Phys., **91**, 8022 (2002).
53) S. Saito, S. Hinata, and M. Takahashi: *IEEE Trans. Magn.*, **50**, 3201205 (2014).
54) K. Yoshida, H. Kakibayashi1 and H. Yasuoka: *J. Appl. Phys.*, **68**, 705 (1990).
55) J. O. Artman: J. Appl. Phys., **61**, 3137 (1987).
56) Y. Maeda, S. Hirono, and M. Asahi: Japan. *J. Appl. Phys.*, **24**, L951 (1985).
57) Y. Maeda and M. Asahi: *J. Appl. Phys.*, **61**, 1972 (1987).
58) H. Suzuki, N. Goda, S. Nagaike, Y. Shiroishi, N. Shige, and N. Tsumita: *IEEE Trans. Magn.*, **27**, 4718 (1991).
59) J .N. Chapman, I. R. McFadyen, and J. P. C. Bernards: *J. Mag. Mag. Mater.*, **62**, 359 (1986).
60) D. I. Rogers, J. N. Chapman, J. P. C. Bcrnalds, and S. B. Luitjens: *IEEE Trans. Magn.*, **25**, 4180 (1989).
61) H. Aoi, F. Tomiyama, Y. Shiroishi, K. Yoshida, and Y. Sugita: *IEEE Trans. Magn.*, **29**, 3715 (1993).
62) H. Aoi, F. Kugiya, R. Tsuchiya, and M. Suzuki: *IEEE Trans. J. Mag. Japan*, **4**, 164 (1989).
63) M. Futamoto: *Tech. Rep. IEICE*, **MR94-81**, 53 (1995).
64) M. Futamoto, N. Inaba, Y. Hrayama, K. Kimoto, and K. Usami: *Tech. Rep. IEICE*, **MR95-49**, 35 (1995).
65) Y. Yahisa, K. Kimoto, K. Usami, Y. Matsuda, J. Inagaki, K. Furusawa, and S. Narishige: *IEEE Trans. Magn.*, **31**, 2836 (1995).
66) Y. Hirayama, M. Futamoto, K. Kimoto, and K. Usami: *IEEE Trans. Magn.*, **32**, 3807 (1996).
67) K. Kimoto, Y. Hirayama, and M. Futamoto: *J. Mag. Mag. Mater.*, **159**, 401 (1996).
68) J. Nakai, A. Kikuchi, M. Kuwabara, T. Sakurai, T. Shimatsu, and M. Takahashi: *IEEE Trans. Magn.*, **31**, 2833 (1995).
69) M. Takahashi, A. Kikuchi, H. Hara, and H. Shoji: *IEEE Trans. Magn.*, **34**, 1573 (1998).
70) M. Futamoto, Y. Honda, and K. Yoshida: *J. Mag. Mag. Mater.*, **74**, 134 (1988).
71) M. Futamoto, Y. Hirayama, Y. Honda, and A. Kikukawa: *NATO Science Series* "Magnetic Storage Systems beyond 2000" ed. by G. C. Hadjipanayis, p. 103, (Kluwer Acad. Pub., Netherlands, 2001).
72) Y. Hirayama, K. Ito, Y. Honda, N. Inaba, and M. Futamoto: *J. Mag. Mag. Mater.*, **193**, 253 (1999).
73) N. Inaba, Y. Uesaka, and M. Futamoto: *IEEE Trans. Magn.*, **36**, 54 (2000).
74) P. F. Carcia, A. D. Meinhaldt, and A. Suna: *Appl. Phys. Lett.*, **47**, 178 (1985).
75) M. Suzuki, H. Awano, N. Inaba, Y. Honda, and M. Futamoto: *J. Mag. Soc. Japan*, **18**, Suppl. No. S1, 451 (1994).
76) B. M. Lairson, J. Perez, and C. Baldwin: *IEEE Trans. Magn.*, **30**, 4014 (1994).
77) L. Wu, N. Honda, and K. Ouchi: *IEEE Trans. Magn.*, **35**, 2775 (1999).
78) Y. Kubota, D. Weller, M-L. Wu, X. Wu, G. Ju, D. Karns, and J. Yu: *J. Mag. Mag. Mater.*, **242-245**, 297 (2002).
79) S. Matsunuma, A. Yano, T. Koda, T. Onuma, H. Yamanaka, and E. Fujita: *IEEE Trans. Magn.*, **40**, 2492 (2004).
80) Y. Ota, N. Tani, M. Ishikawa, T. Yamada, K. Nakamura and A. Itoh: *IEEE Trans. Magn.*, **MAG-20**, 768 (1984).
81) T. Sato and T. Kitamura: *IEEE Trans. J. Mag. Japan*, **TJMJ-1**, 765 (1985).
82) K. Yoshida and T. Takayama: *J. Mag. Mag. Mater.*, **82**, 228 (1989).
83) T. Hikosaka, T. Komai, and Y. Tanaka: *IEEE Trans. Magn.*, **30**, 4026 (1994).
84) Y. Tanaka and T. Hikosaka: *J. Magn. Magn. Mater.*, **235**, 253 (2001).
85) A. Takeo, S. Oikawa, T. Hikosaka, and Y. Tanaka: *IEEE Trans. Magn.*, **36**, 2378 (2000).
86) Y. Tanaka: *IEEE Trans. Magn.*, **41**, 2834 (2005).
87) T. Handa, Y. Takahashi, R. Araki, and M. Futamoto: *J. Mag. Soc. Japan*, **32**, 260 (2008).
88) M. Futamoto, T. Handa, and Y. Takahashi: *IEEE Trans. Magn.*, **44**, 3488 (2008).
89) M. Futamoto, T. Handa, and Y. Takahashi: *J. Phys. Conf. Ser.*, **200**, 102001 (2010).
90) H. Weinforth, Ch. Somsen, B. Rellinghaus, A. Carl, E. F. Wassermann, and D. Weller: *IEEE Trans. Magn.*, **34**, 1132 (1998).
91) T. Oikawa, M. Nakamura, H. Uwazumi, T. Shimatsu, H. Muraoka, and Y. Nakamura: *IEEE Trans. Magn.*, **38**, 1976 (2002).
92) J. Ariake, T. Chiba, and N. Honda: *IEEE Trans. Magn.*, **41**, 3142 (2005).
93) T. Chiba, J. Ariake, and N. Honda: *J. Mag. Mag. Mater.*, **287**, 167 (2005).
94) S. Iwasaki, Y. Nakamura, and K. Ouchi: *IEEE Trans. Magn.*, **MAG-15**, 1456 (1979).
95) S. B. Luitjens, C. P. G. Schrauwen, J. P. C. Bernards, and V. Zieren: *IEEE Trans. Magn.*, **MAG-21**, 1438 (1985).
96) T. Ando and T. Nishihara: *J. Mag. Soc. Japan*, **15**, Suppl. S2, 1019 (1991).
97) Y. Honda, K. Tanahashi, Y. Hirayama, A. Kikukawa, and M. Futamoto: *IEEE Trans. Magn.*, **37**, 1315 (2001).

98) Y. Honda, A. Kikukawa, Y. Hirayama, and M. Futamoto:, *IEEE Trans. Magn.*, **36**, 2399 (2000).

99) A. Kikukawa, Y. Honda, Y. Hirayama, and M. Futamoto: *IEEE Trans. Magn.*, **36**, 2402 (2000).

100) A. Kikukawa, K. Tanahashi, Y. Honda, Y. Hirayama, and M. Futamoto: *IEEE Trans. Magn.*, **37**, 1602 (2001).

101) R. Mukai, T. Uzumaki, and A. Tanaka: *IEEE Trans. Magn.*, **41**, 3169 (2005).

102) K. Tang, X. Bian, G. Choe, K. Takano, M. Mirzamaani, G. Wang, J. Zhang, Q.-F. Xiao, Y. Ikeda, J. R. Jamtgaard, and X. Xu: IEEE Trans. Magn., 45, 786 (2009).

103) J. A. Thornson: *J. Vac. Sci. Technol.*, **A4** (6), 3059 (1986).

104) Y. Sonobe, H. Muraoka, K. Miura, Y. Nakamura, K. Takano, A. Moser, H. Do, B. K. Yen, Y. Ikeda, N. Supper, and W. Weresin: *IEEE Trans. Magn.*, **38**, 2006 (2002).

105) Y. Sonobe, K. K. Tham, L. Wu, T. Umezawa, C. Takasu, J. A. H. Dumaya, T. Onoue, P. Leo, and M. Liau: *IEEE Trans. Magn.*, **42**, 2351 (2006).

106) Y. Honda, M. Futamoto, T. Kawasaki, K. Yoshida, M. Koizumi, F. Kugiya, and A. Tonomura: *Japan. J. Appl. Phys.*, **26**, L923 (1987).

107) K. Yoshida, Y. Honda, T. Kawasaki, M. Koizumi, F. Kugiya, M. Futamoto, and A. Tonomura: *IEEE Trans. Magn.*, **MAG-23**, 2073 (1987).

108) K. Yoshida, Y. Honda, M. Futamoto, T. Kawasaki, S. Hasegawa, and A. Tonomura: *J. Mag. Soc. Japan*, **15**, Suppl. No. S2, 463 (1991).

109) K. Ouchi and S. Iwasaki: *IEEE Trans. Magn.*, **MAG-18**, 1110 (1982).

110) T. Kohashi, M. Konoto, A. Nakamura, R. Araki, and K. Koike: *Digest of Intermag 2006*, HD-04 (2006).

111) J. P. C. Bernards and A. J. den Boef: *IEEE Trans. Magn.*, **26**, 1515 (1990).

112) Y. Honda, S. Hosaka, A. Kikukawa, S. Tanaka, Y. Matsuda, M. Suzuki, and M. Futamoto: *Japan. J. Appl. Phys.*, **31**, L1061 (1992).

113) M. Futamoto and Y. Honda: *J. Mag. Soc. Japan*, **18**, Suppl. No. S1, 485 (1994).

114) G. Binning, C. F. Quate, Ch. Gerber: *Phys. Rev. Lett.*, **56**, 930 (1986).

115) K. Nagano, K. Tobari, K. Soneta, M. Ohtake, and M. Futamoto: *J. Mag. Soc. Japan*, **36**, 109 (2012).

116) M. Futamoto, T. Hagami, S. Ishihara, K. Soneta, and M. Ohtake: *Key Eng. Mater.*, **543**, 35 (2013).

117) S. Ishihara, M. Ohtake, and M. Futamoto: *J. Mag. Soc. Japan*, **37**, 255 (2013).

118) M. Futamoto, T. Hagami, S. Ishihara, K. Soneta, and M. Ohtake: *IEEE Trans. Magn.*, **49**, 2748 (2013).

119) M. Futamoto and M. Ohtake: *Key Eng. Mater.*, **644**, 189 (2015).

120) L. Gao, L. P. Yue, T. Yokota, R. Skomski, S. H. Liou, H. Takahoshi, H. Saito, and S. Ishio: *IEEE Trans. Magn.*, **40**, 2194 (2004).

121) N. Amos, A. Lavrenov, R. Fernandez, R. Ikkawi, D. Litvinov, and S. Khizroev: *J. Appl. Phys.*, **105**, 07D526 (2009).

122) W. Lu, Z. Li, K. Hatakeyama, G. Egawa, S. Yoshimura, and H. Saito: *J. Appl. Phys.*, **96**, 143104 (2010).

123) K. Soneta, M. Ohtake, and M. Futamoto: *J. Mag. Soc. Japan*, **37**, 107 (2013).

124) T. Hagami, M. Ohtake, and M. Futamoto: *J. Mag. Soc. Japan*, 37, 231 (2013).

125) S. Ishihara, M. Ohtake, and M. Futamoto: *EPJ Web Conf.*, **40**, 01002, (2013).

126) M. Futamoto: *ECS Trans.*, **50**, 59 (2013).

127) T. Suzuki, N. Honda, and K. Ouchi: *Tech. Rept. IEICE*, **MR97-16**, 53 (1997)

128) D. Weller and A. Moser: *IEEE Trans. Magn.*, **35**, 4423 (1999).

129) T. Burkert, L. Nordström, O. Eriksson, and O. Heinonen: *Phys. Rev. Lett.*, **93**, 027203 (2004).

130) Y. Nukaga, M. Ohtake, F. Kirino, and M. Futamoto: *IEEE Trans. Magn.*, **44**, 2891 (2008).

131) M. Ohtake, Y. Nukaga, F. Kirino, and M. Futamoto: *J. Appl. Phys.*, **105**, 07C315 (2009).

132) O. Yabuhara, M. Ohtake, Y. Nukaga, F. Kirino, and M. Futamoto: *J. Phys. Conf. Ser.*, **200**, 082026 (2010).

133) M. Ohtake, O. Yabuhara, Y. Nukaga, F. Kirino, and M. Futamoto: *J. Appl. Phys.*, **107**, 09A708 (2010).

134) T. Yanagawa, M. Ohtake, F. Kirino, and M. Futamoto: *EPJ Web Conf.*, **40**, 06007 (2013).

135) M. Yamada, Y. Hotta, T. Yanagawa, M. Ohtake, F. Kirino, and M. Futamoto: *IEEE Trans. Magn.*, **50**, 2101604 (2014).

136) M. Yamada, T. Yanagawa, Y. Hotta, M. Ohtake, F. Kirino, and M. Futamoto: *EPJ Web Conf.*, **75**, 04010 (2014).

137) M. Yamada, Y. Hotta, A. Suzuki, M. Ohtake, M. Futamoto, F. Kirino, and N. Inaba: *Digest 38th Conf. Mag. Soc. Japan*, 2aB-03, p.18 (2014).

138) M. Seifert, V. Neu, and L. Schultz: *Appl. Phys. Lett.*, **94**, 022501 (2009).

139) M. Ohtake, Y. Nukaga, F. Kirino, and M. Futamoto: *J. Cryst. Growth*, **311**, 2251 (2009).

140) B. N. Engel, C. D. England, R. A. Van Leeuwen, M. H. Wiedmann, and C. M. Falco: *Phys. Rev. Lett.*, **67**, 1910 (1991).

141) H. Ohmori and A. Maesaka: *J. Mag. Soc. Japan.*, **26**, 224 (2002).

142) K. Tobari, M. Ohtake, K. Nagano, and M. Futamoto: Japan. *J. Appl. Phys.*, **50**, 073001 (2011).

143) K. Tobari , M. Ohtake, K. Nagano, and M. Futamoto: *Thin Solid Films*, **519**, 8384 (2011).

144) K. Tobari, M. Ohtake, K. Nagano, and M. Futamoto: *J. Mag. Mag. Mater.*, **324**, 1059 (2012).

145) M. Ohtake, K. Tobari, and M. Futamoto: *IEICE Trans. Electron.*, **E96-C**, 1452 (2013).

146) H. Okamoto: Phase Diagrams for Binary Alloys, p. 255 (Materials Park, OH, ASM International, 2000).

147) S. Iwata, S. Yamashita, and S. Tsunashima: *IEEE Trans. Magn.*, **32**, 3670 (1997).

148) G. F. Hughes: Patterned Media in "The Physics of Ultra-High-Density Magnetic Recording", p. 205 (Springer, New York, 2002).

149) E. Suharyadi, S. Natsume, T. Kato, S. Tsunashima, and S. Iwata: *Trans. Magn. Soc, Japan*, **5**, 125 (2005).

150) K. Takenaka, N. Saidoh, N. Nishiyama, M. Ishimaru, M. Futamoto, and A. Inoue: *J. Mag. Mag. Mater.*, **324**, 1444 (2012).

151) S. Chikazumi et al. ed.: Handbook of Magnetic Materials, (Asakura Shoten, Tokyo, 2006).

152) J. M. D. Coey: Magnetism and Magnetic Materials, (Chambridge University Press, New York, 2009).

153) A. Itabashi, M. Ohtake, F. Kirino, and M. Futamoto: *IEICE Tech. Rept.*, **MR2013-7**, 7 (2013).

154) Z. L. Jun, N. S. Hua, and Z. J. Hua: *ArXiv* 1309.0298, pp.1-14 (2013).

155) R. S. Bandhu and R. Sooryakumar, R. F. C Farrow, D. Weller, M. F. Toney, and T. A. Rabedeau: *J. Appl. Phys.*, **91**, 2737 (2002)

156) G. R. Harp, D. Weller, T. A. Rabedeau, R. F. C. Farrow, and M. F. Toney: *Phys. Rev. Lett.*, **71**, 2493 (1993).

157) T. Suzuki, N. Honda, and K. Ouchi: *J. Mag. Soc. Japan*, **21,** S2, 177 (1997).

158) T. Suzuki, T. Kiya, N. Honda, and K. Ouchi: *IEEE Trans. Magn.*, **36**, 2417 (2000).

159) T. Suzuki and K. Ouchi: *IEEE Trans. Magn.*, **37**, 1283 (2001).

160) D. E. Laughlin, S. Kumar, Y. Peng, and A. G. Roy: *IEEE Trans. Magn.*, **41**, 719 (2005).

161) D. Weller, G. Parker, O. Mosendz, E. Champion, B. Stipe, X. Wang, T. Klemmer, G. Ju, and A. Ajan: *IEEE Trans. Magn.*, **50**, 3100108 (2014).

162) D. Suzuki, M. Ohtake, F. Kirino, and M. Futamoto: *IEEE*

Trans. Magn., **48**, 3195 (2012).
163) M. Ohtake, S. Ouchi, F. Kirino , and M. Futamoto: *IEEE Trans. Magn.*, **48**, 3595 (2012).
164) D. Suzuki, M. Ohtake, S. Ouchi, F. Kirino, and M. Futamoto: *J. Mag. Soc. Japan*, **36**, 336 (2012).
165) D. Suzuki, M. Ohtake, F. Kirino, and M. Futamoto: *J. Mag. Soc. Japan*, **37**, 179 (2013).
166) M. Ohtake, D. Suzuki, F. Kirino, and M. Futamoto: *ECS Trans.,* **50**, 69 (2013).
167) D. Suzuki, M. Ohtake, F. Kirino, and M. Futamoto: *EPJ Web Conf.*, **40**, 11003 (2013).
168) M. Ohtake, D. Suzuki, F. Kirino, and M. Futamoto: *IEICE Trans. Electron.*, **E96-C**, 1460 (2013).
169) M. Ohtake, D. Suzuki, and M. Futamoto: *J. Appl. Phys.*, **115**, 17C116 (2014).
170) D. Suzuki, M. Ohtake, F. Kirino, and M. Futamoto: *J. Appl. Phys.*, **115**, 17C120 (2014).
171) M. Ohtake, D. Suzuki, F. Kirino, and M. Futamoto: *EPJ Web Conf.*, **75**, 06003 (2014).
172) M. Ohtake, D. Suzuki, M. Futamoto, F. Kirino, and N. Inaba: *J. Mag. Soc. Japan*, **39**, 15 (2015).
173) K. Sato, B. Bian, T. Hanada, and Y. Hirotsu: *Scripta Mater.*, **44**, 1389 (2001).
174) K. Sato, B. Bian, and Y. Hirotsu: *J. Appl. Phys.*, **91**, 8516 (2002).
175) A. Itabashi, M. Ohtake, S. Ouchi, F. Kirino, and M. Futamoto: *J. Mag. Soc. Japan*, **37**, 358 (2013).
176) Y. Numata, A. Itabashi, M. Phtake, F. Kirino, and M. Futamoto: *IEEE Trans. Magn.*, **50**, 210304 (2014).
177) A. Itabashi, M. Ohtake, S. Ouchi, F. Kirino, and M. Futamoto: *IEEE Trans. Magn.*, **48**, 3203 (2012).
178) A. Itabashi, M. Ohtake, F. Kirino, and M. Futamoto: *EPJ Web Conf.*, **75**, 06012 (2014).
179) M. Ohtake, A. Itabashi, M. Futamoto, F. Kirino, and N. Inaba: *Key Eng. Mater.*, **644**, 227 (2015).
180) M. Ohtake, A. Itabashi, M. Futamoto, F. Kirino, and N. Inaba: *IEEE Trans. Magn.*, **51**, 2100904 (2015).
181) M. Futamoto, M. Nakamura, M. Ohtake, N. Inaba, and T. Shimotsu: *AIP Adv.*, **6**, 085302 (2016).
182) Y. Numata, M. Ohtake, M. Futamoto, F. Kirino, and N. Inaba: *Abst. 38th Conf. Mag. Soc. Japan.*, 4aE-10, p.289 (2014).
183) M. Nakamura, R. Ochiai, M. Ohtake, M. Futamoto, F. Kirino, and N. Inaba: *IEICE Tech. Rep.,* **MR2016-14**, 7 (2016).
184) J. A. Venables: Introduction to Surface and Thin Film Processes, (Cambridge Univ. Press, Cambridge, 2000).
185) M. Ohtake, S. Ouchi, F. Kirino, and M. Futamoto: *J. Appl. Phys.*, **111**, 07A708 (2012).
186) L. S. Huang, J. F. Hu, G. M. Chow, and J. S. Chen: *J. Appl. Phys.*, **109**, 063910 (2011).
187) I. Takekuma, H. Nemoto, H. Matsumoto, S. Ito, J. Sayama, A. Hirotsune, and Y. Hirayama: *J. Appl. Phys.*, **111**, 07B708 (2012).
188) K. F. Dong, H. H. Li, Y. G. Peng, G. Ju, G. M. Chow, and J. S. Chen: *Appl. Phys. Lett.*, **104**, 192404 (2014).
189) T. Young: *Philos. Trans. R. Soc. Lond.*, **95**, 65 (1805).
190) T. Shimizu, M. Ohtake, M. Futamoto, F. Kirino, and N. Inaba, *IEEE Trans. Magn.* **53** (2017) (to appear).
191) M. Ohtake, A. Itabashi, M. Futamoto, F. Kirino, and N. Inaba: *J. Mag. Soc. Japan*, **39**, 167 (2015).
192) Y. Noguchi, M. Ohtake, M. Futamoto, and N. Inaba: *J. Mag. Mag. Mater.*, **410**, 81 (2016).

Received May 05, 2017; Revised June 28, 2017; Accepted August 17, 2017